COMMUNICATIONS IN SCIENCE AND TECHNOLOGY
Homepage: cst.kipmi.or.id

The effect of ultrasound-assisted enzymatic hydrolysis (UAEH) on the physicochemical properties and bioactivity of edible swiftlet's nest hydrolysates

Nita Kusumawati[a], Pirim Setiarso[a,*], Sunu Kuntjoro[b], Ita Fatkhur Romadhoni[c], Gina Noor Djalilah[d], Khofifatul Rahmawati[a], Senja Salzanabila Putri Perdana[a], Achmad Naufal Al Hafidl[a], Amirul Mu'minin[a], Safira Keysa Dewayanti[a], Anandatya Ramdhan Achmad Al Manfaluty[a], Shafira Basri[a], Nailah Clarinta Artanti[a], Firnanda Amelia Wulandari[a], Aprilia Putri Nur Afifatun Nisak[a], Muhammad Zaky Fachriansyah[a]

[a]*Department of Chemistry, Universitas Negeri Surabaya, Surabaya 60231, Indonesia*
[b]*Department of Biology, Universitas Negeri Surabaya, Surabaya, 60231, Indonesia*
[c]*Department of Culinary Arts, Universitas Negeri Surabaya, Surabaya, 60231, Indonesia*
[d]*Department of Medical Education, Universitas Muhammadiyah Surabaya, Surabaya, 60113, Indonesia*

Article history:
Received: 28 April 2026 / Received in revised form: 21 June 2026 / Accepted: 22 June 2026

Abstract

This study investigates the effect of ultrasound-assisted enzymatic hydrolysis (UAEH) compared with non-hydrolyzed samples on the physicochemical properties and bioactivity of edible swiftlet's nest (ESN) co-product hydrolysates using bromelain under optimized processing conditions. ESN was subjected to UAEH treatment (40 °C, pH 7.0, 40 kHz) followed by freeze-drying. The results showed that hESN-C achieved the highest yield (62.13%) and degree of hydrolysis (37.95%), while hESN-CP gave the lowest (28% yield, 9.57% degree of hydrolysis). FTIR spectroscopy confirmed the retention of key glycoprotein functional groups across all hydrolysate fractions: characteristic O–H/N–H stretching vibrations at 3270-3272 cm^{-1}, Amide I at 1630-1631 cm^{-1}, and Amide II at 1526-1537 cm^{-1}, together with glycan-associated C–O/C–N stretching vibrations, indicating selective peptide bond cleavage by bromelain without disruption of glycosidic linkages and preservation of the carbohydrate architecture in the resulting bioactive glycopeptides. HPLC qualitatively confirmed sialic acid retention in all fractions (retention time 6-7 min). Amino acid profiling revealed complete essential amino acid profiles in all samples, with the highest concentrations in hESN-C dominated by L-valine (36,507.33 mg/kg), L-proline (37,083.32 mg/kg), and L-serine (37,635.48 mg/kg). Fatty acid analysis identified oleic acid (0.1491%) and linoleic acid (0.0428%) as the predominant unsaturated fatty acids, particularly in hESN-CP. Particle size analysis demonstrated that UAEH produced smaller, more uniformly distributed nanoparticles (14.17-27.03 nm) with low polydispersity indices (<0.3). Scanning electron microscopy revealed distinct morphological differences: hESN-C and hESN-D exhibited homogeneous laminar structures, whereas hESN-CP displayed heterogeneous porous morphology attributed to keratin from feather residues. UAEH treatment significantly increased soluble protein content (hESN-C: 1.246 µg/µL; hESN-CP: 0.844 µg/µL) and DPPH radical scavenging activity (up to 10.70% for hESN-CP) relative to non-hydrolyzed controls. Heavy metal concentrations (Hg: 0.0172–0.0236 mg/L; Cd: 0.1194–0.1444 mg/L; Pb: 0.11–1.4 mg/L) remained within Chinese safety thresholds, and water activity was reduced to safe levels (<0.60). Collectively, these results demonstrate that UAEH is an effective and sustainable strategy for valorizing ESN co-products into physicochemically improved, bioactive glycopeptide hydrolysates with potential as functional food ingredients. Future studies employing quantitative in vitro bioactivity assays and in vivo validation are warranted to substantiate broader health-benefit claims.

Keywords: Ultrasound-assisted enzymatic hydrolysis; edible swiftlet nest co-product hydrolysates; bromelain; freeze-drying; bioactivity

1. Introduction

Global production of edible swiftlet's nest (ESN) has continued to rise significantly, with international trade volumes projected to reach substantial levels by 2030 [1]. Indonesia, as one of the largest producers and exporters, maintains approximately 70-80% of the world's ESN exports annually [2]. This expansion inevitably generates large volumes of co-products, including broken nests, feathers, and cleaning residues, estimated at approximately 30% of total production in Indonesian swiftlet farming [3]. These co-products are largely underutilized, posing both economic and environmental burdens that call for sustainable valorization approaches

* Corresponding author.
Email: pirimsetiarso@unesa.ac.id
https://doi.org/10.21924/cst.11.1.2026.1974

aligned with circular bioeconomy principles, particularly given China's increasingly stringent import standards regarding protein content, sialic acid levels, and overall product purity [4].

ESN co-products retain substantial concentrations of glycoproteins, essential amino acids, and bioactive compounds, most notably sialic acid (N-acetylneuraminic acid). ESN glycoproteins predominantly adopt mucin-type structures with molecular weights of 10-100 kDa, conferring structural rigidity and functional bioactivity [1,5]. Their high protein content (approximately 50-60% dry weight) and intact glycopeptide architecture make them a promising starting material for functional ingredient development [6,2]. However, the dense, cross-linked glycoprotein matrix presents a fundamental barrier to conventional enzymatic hydrolysis: limited enzyme accessibility to cleavage sites results in incomplete hydrolysis, low yields, and diminished bioactivity of the resulting hydrolysates [7,8]. Standard extraction approaches are further constrained by prolonged processing times at elevated temperatures, which risk thermal degradation of heat-sensitive bioactive components, and by poor control over the molecular weight distribution of the resulting glycopeptides [8,9].

Ultrasound-assisted enzymatic hydrolysis (UAEH) offers a mechanistically distinct solution to these limitations. Acoustic cavitation, generated by ultrasonic irradiation, produces localized zones of extreme pressure and temperature upon bubble collapse, physically disrupting the compact glycoprotein matrix and substantially increasing the solvent-accessible surface area for enzymatic attack [10]. Unlike conventional pre-treatment, cavitation actively unfolds mucin-type glycoprotein structures, exposing previously inaccessible peptide bonds to enzymatic cleavage, while ultrasound-induced microstreaming enhances mass transfer at the enzyme-substrate interface [11]. These synergistic effects collectively yield higher degrees of hydrolysis, lower molecular weight glycopeptide fractions, and superior bioactivity relative to enzymatic hydrolysis alone [10,11]. Bromelain is particularly well-suited for this application owing to its broad endo- and exopeptidase specificity, stability under mild processing conditions, and demonstrated effectiveness in cleaving peptide bond environments characteristic of ESN mucin-type glycoproteins [9,12,13].

Despite these advantages, the application of UAEH specifically to ESN co-products, as opposed to cleaned nest grades, remains poorly understood. ESN co-products contain higher levels of residual impurities (feathers, saliva contaminants, and mineral deposits), lower glycoprotein purity, and more heterogeneous matrix structures that may alter cavitation dynamics and enzyme-substrate interaction kinetics [7,14]. Furthermore, prior studies on ESN hydrolysates have largely reported physicochemical characterization without establishing mechanistic linkages between UAEH parameters, molecular-level structural changes in the glycoprotein matrix, and the resulting functional bioactivities of hydrolysates [7,10,11]. Understanding these mechanistic relationships, particularly how cavitation-induced structural disruption translates into changes in peptide bond accessibility, degree of hydrolysis, molecular weight distribution, and antioxidant activity, is essential for rational process design and the development of standardized, scalable valorization protocols for ESN co-products.

After hydrolysis, freeze-drying is used as the final processing step to produce a stable, ready-to-use powdered product. Although it is pricier than conventional drying, as reported by Yeo et al. (2023), freeze-drying prevents thermal degradation of heat-sensitive bioactive compounds, preserves the structural integrity of glycopeptides, and yields hydrolysates with superior reconstitution properties [11], making it suitable for functional food and nutraceutical applications where bioactivity retention is critical.

Based on these considerations, this study aims to investigate the mechanistic basis and process outcomes of ultrasound-assisted enzymatic hydrolysis applied to ESN co-products, with a focus on establishing relationships between UAEH-induced structural modifications of the glycoprotein matrix and the physicochemical properties and bioactivities of the resulting freeze-dried hydrolysates. The scientific novelty of this work lies in three contributions. Elucidating the mechanistic role of acoustic cavitation in disrupting the compact mucin-type glycoprotein architecture of ESN co-products and its downstream effects on hydrolysate quality; systematically characterizing how the distinct compositional profile of ESN co-products, relative to cleaned nest grades, modulates UAEH efficiency and bioactivity outcomes; and establishing structure-function relationships between glycopeptide molecular characteristics and antioxidant bioactivity in co-product-derived hydrolysates. Comprehensive characterization was conducted using FTIR spectroscopy, amino acid and fatty acid profiling, HPLC analysis, scanning electron microscopy (SEM), particle size analysis, soluble protein quantification, viscosity measurement, antioxidant activity assay, heavy metal analysis, whiteness index determination, and water activity measurement. The findings are expected to provide mechanistic scientific insights that advance rational process design for ESN co-product valorization as functional ingredients, while contributing to waste reduction and sustainable development of the ESN industry in support of a circular bioeconomy.

2. Materials and Methods

2.1. Materials

Raw Edible Swiftlet Nest's (ESN) were obtained from suppliers in Lombok, Indonesia. Several chemicals required for ESN preparation and extraction included distilled water for preparation, bromelain enzyme from pineapple stem (≥99.9% purity, Sigma Aldrich, USA) for glycoprotein hydrolysis, sodium hydroxide (NaOH) (96% purity; Merck, Singapore) and hydrochloric acid (HCl) (≥37% purity; Fluka, Austria) for pH adjustment during enzymatic-assisted extraction (EAE).

2.2. Methods

The ESN extraction procedure followed the approaches described by Chong et al. (2022) and Tang & Koh (2023), consisting of four main stages: pre-treatment, glycoprotein extraction, enzymatic hydrolysis, and drying [12,15,16]. The process involved maceration of ESN, ultrasonic-assisted extraction, bromelain-based hydrolysis, and final freeze-drying to obtain the dried ESN hydrolysate.

2.2.1. Pre-treatment

The raw ESN samples (ESN-C, ESN-D, and ESN-CP) were finely ground to obtain a homogeneous powder. 15 g of this powder was dissolved in 750 mL of distilled water, producing an initial mixture that was subsequently macerated in a refrigerator at 4 ± 1 °C for 24 hours to allow hydration. The resulting slurry was subjected to controlled heating in a water bath at 90 °C for 30 minutes, as shown in Fig. 1.

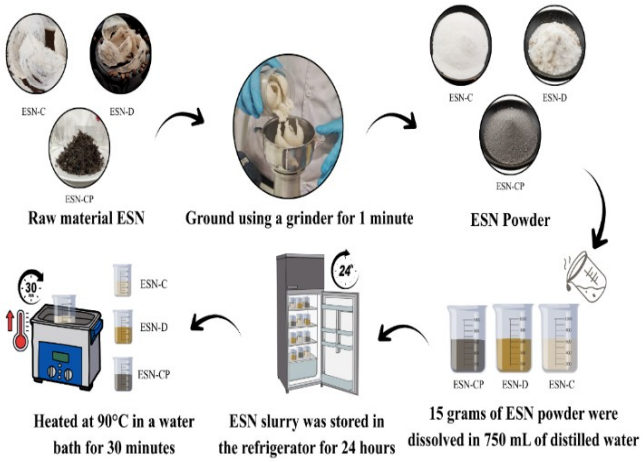

Fig. 1. Pre-treatment process for the preparation of ESN sample

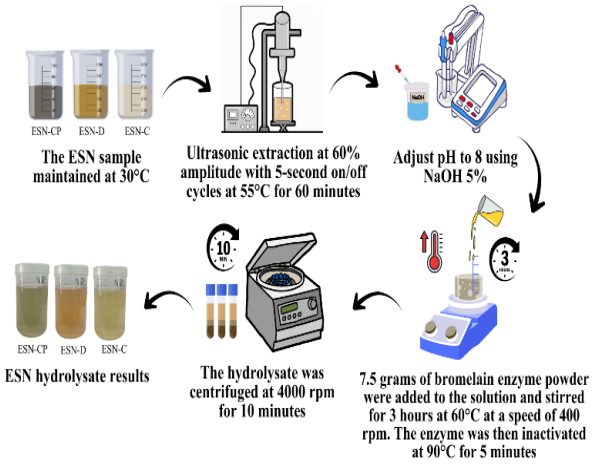

Fig. 2. Enzymatic-assisted extraction process for the ESN hydrolysate

2.2.2. Ultrasonic-assisted extraction (UAE) and enzymatic-assisted extraction (EAE) of ESN glycoproteins into glycopeptides

The glycoprotein extraction using the UAE method was initiated with the ESN samples maintained at 30 °C, followed by ultrasonic treatment using a Guangzhou Fo Bun UH-3000W ultrasonic homogenizer at 60% amplitude with 5-second on/off pulse cycles for 60 minutes, while ensuring that the extraction temperature remained at 55 °C. Subsequently, the ESN extract was adjusted to pH 8 using 5% NaOH and hydrolyzed into glycopeptides using the bromelain enzyme at a 1:100 (enzyme:solvent) ratio, corresponding to 7.5 g of enzyme powder. The enzymatic reaction was carried out at 60 °C for 3 h with continuous stirring at 400 rpm, followed by enzyme inactivation at 90 °C for 5 min. The resulting mixture was centrifuged at 4000 rpm for 10 min to obtain the clear ESN hydrolysate, as shown in Fig. 2. In this study, the non-hydrolyzed raw ESN samples (ESN-C, ESN-D, and ESN-CP) served as negative baseline controls, enabling direct quantitative comparison of the overall UAEH treatment effect across all measured physicochemical and bioactivity parameters. The UAEH processing conditions applied (40 kHz, pH 7.0, 40 °C, and bromelain at a 1:100 ratio) were adopted based on parameters previously validated and optimized in prior studies for their combined synergistic effect, whereby ultrasonic cavitation enhances substrate accessibility for enzymatic action beyond what either treatment achieves independently [2,17].

2.2.3. Drying method

750 mL of ESN hydrolysate was poured into a stainless-steel tray and frozen at -4 °C for 24 hours as a pre-treatment step. The frozen hydrolysate was processed by freeze-drying at -60 ± 2 °C under a pressure of 0.30-0.36 Pa using a Guangzhou Fo Bun KFD-4 Freeze Dryer (China). The resulting freeze-dried ESN hydrolysate formed brittle sheet-like solids, which were later pulverized into fine hydrolysate powder, as shown in Fig. 3.

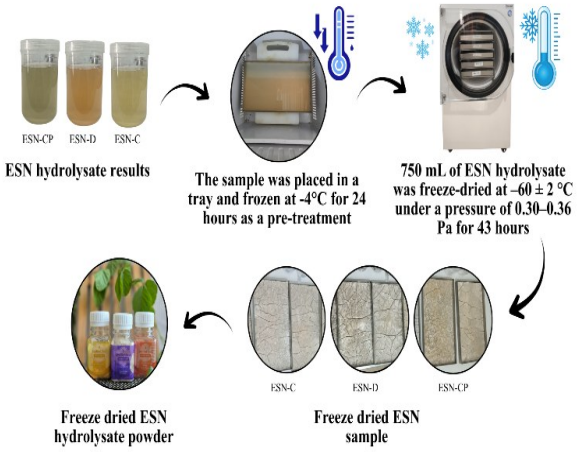

Fig. 3. Freeze drying process

2.2.4. Yield

Yield and weight loss were determined by following Eq. 1-3 [18,19].

$$\%\text{Yield} = \frac{W_{fk}}{W_{ik}} \times 100\% \quad (1)$$

Meanwhile, weight loss is calculated using formula 2-3 as follows:

$$\%\text{loss} = \frac{W_{ik} - W_{fk}}{W_{fk}} \times 100\% \quad (2)$$

$$\%\text{total weight loss} = \frac{W_I - W_{fk}}{W_i} \times 100\% \quad (3)$$

where W_{ik} and W_{fk} refer to the weight of wet and dry ESN, respectively, while W_i is the weight of ESN.

2.2.5. Fourier transform infrared (FTIR) analysis

The functional groups of ESN powder obtained from freeze-drying using UAEH method using bromelain enzyme were analyzed using the FTIR spectrophotometer (Perkin Elmer Spectrum Two). Spectral data were collected in transmission mode at 4000-500 cm^{-1}.

2.2.6. Degree of hydrolysis analysis

To measure the hydrolysis level, the ESN hydrolysates were analyzed via voltammetry using a 797 VA Computrace system (Metrohm, Switzerland), employing an adsorptive stripping voltammetry (AdSV) mode that quantifies the electrochemical signal of free amino groups released upon peptide bond cleavage. The samples were prepared by dilution to 10 ppm with KCl added as an Ionic Strength Adjuster (ISA) at 50-100 times the sample concentration. The degree of hydrolysis was subsequently determined by evaluating the height increase of the reduction peak in the resulting voltammogram. The AdSV approach quantifies the same chemical species (free amine groups liberated upon peptide bond cleavage) via its detection transducer (electrochemical reduction signal), thereby yielding a DH index that is physically equivalent to the ratio of cleaved peptide bonds to total peptide bonds. The VA Computrace system (Metrohm 797) has been previously applied by Afifah et al. (2024) for protein and peptide analysis in food hydrolysate matrices, further supporting its applicability in the present context [1].

$$\mathrm{DH}\ (\%) = \frac{|I_S| - |I_M|}{|I_M|} \times 100\% \quad (4)$$

Where I_S and I_M refer to the sample current and maceration current.

2.2.7. Profiling amino acid & fatty acid with gas chromatography-mass spectrometry (GC-MS)

Amino acid content was analyzed using a GC-MS system (Agilent 7820A GC, 5977E MSD) in EI mode (70 eV) with helium carrier gas at 1 mL min^{-1}. 1 µL derivatized sample was injected in split mode (20:1). The MS operated with a source temperature of 230 °C and quadrupole temperature of 150 °C. The GC oven was programmed from 100 °C to 325 °C through multiple ramps (total run time 37 min). Data were acquired in full scan mode (45-750 Da) and processed with MassHunter software. Compounds were identified using NIST library matching and quantified using calibration curves based on amino acid/internal standard peak area ratios [20].

2.2.8. Sialic acid

Qualitative testing of sialic acid in hydrolysate solutions was performed using chromatography with HPLC (*Agilent interface 35900E*). A 20 µL sample solution with a concentration of 2 ppm was taken and injected directly into the injection port of the HPLC device. Separation began with a flow rate setting of 0.5 mL/minute.

2.2.9. Soluble protein

The soluble protein content was analyzed using the Bradford assay. 1 g protein sample was dissolved to a concentration of 20 g/100 mL, homogenized, and centrifuged at 3200 rpm for 10 minutes to obtain the supernatant. 100 µL of the supernatant was mixed with 5 mL Bradford reagent (Coomassie Brilliant Blue G-250) and incubated for 15 minutes before measuring its absorbance at 595 nm. Protein concentration was determined using a BSA (Bovine Serum Albumin) calibration curve at a concentration of 2 mg/ml [21].

2.2.10. Viscosity

Viscosity was measured using an NDJ-9S viscometer by maintaining the sample at 25 °C in a container ≥60 mm in diameter. Spindle No. 1 was immersed to the marked line and operated at 12 rpm for 3 minutes. After the reading stabilized, the viscosity value (mPa·s) was noted, and the instrument was stopped and the spindle removed.

2.2.11. Antioxidant activities of ESN hydrolysates

Determination of antioxidant activity using DPPH reagent (2,2-Diphenyl-1-picrylhydrazyl) reacted with ESN hydrolysate. DPPH reagent with a concentration of 300 ppm was prepared using 2.1 mg of DPPH powder in 7 mL of methanol. Next, an ascorbic acid solution was prepared as a positive control and a hydrolysate sample solution at a concentration of 100 ppm, which was prepared using 0.4 mg in 4 mL of methanol. Absorbance measurements were then performed by taking 2 mL samples of hydrolysate, ascorbic acid, and methanol (as a negative control) and mixing them with 0.5 mL of DPPH reagent for each solution. A sample control solution was also prepared by taking 2 mL of the sample solution in 0.5 mL of methanol. All solutions to be measured were incubated at 25oC for 30 minutes. They were then measured at a wavelength of 517 nm using a UV-Vis spectrophotometer. The percentage of inhibition was calculated using the following formula:

$$\%\mathrm{i} = \frac{(\text{Abs.Negatve control- Abs.Blank})-(\text{Abs.Sample-Abs.Sample control})}{(\text{Abs. Negative control - Abs. Blank})} \times 100\% \quad (5)$$

In theory, a higher percentage of inhibition indicates stronger antioxidant activity [22].

2.2.12. Atomic absorption spectrofortrometry (AAS)

Heavy metals (Pb, Cd, and Hg) in the hESN samples were subjected to an acid digestion procedure using concentrated HCl. 1.0 g portion of oven-dried hydrolysate was treated with concentrated HCl [23], and the resulting digested solution was subsequently measured using a Shimadzu AA-7000 AAS at the respective wavelengths (Hg 253.7 nm, Cd 228.8 nm, Pb 217.0 nm). Calibration curves were prepared for each metal using standard solutions at concentrations of 0.1, 0.5, 1, 3, and 5 mg/L, which were used to determine the concentrations of Pb, Cd, and Hg in the samples.

2.2.13. Particle size analysis (PSA)

The particle size of ESN hydrolysate was analyzed using a BK-802N DLS Nano Particle Size Analyzer (Biobase) with a 532 nm laser. 400 ppm solution was prepared by dissolving 10 mg of hydrolysate powder in distilled water to a final volume of 25 mL. The prepared sample was transferred into a clean quartz cuvette and measured at room temperature. The instrument recorded the hydrodynamic particle size distribution, and the results were expressed as *Polydispersity Index* (PdI) and diameter size (nm).

2.2.14. Scanning electron microscopy (SEM)

To determine the surface morphology, size, and particle distribution of ESN hydrolysate particles, analysis was carried out using a Scanning Electron Microscope (*Thermo Fisher Scientific-Phenom P-Series*) at magnifications of 500x, 1.000x, 10.000x, 30.000x.

2.2.15. Whiteness index

Whiteness evaluation was conducted using a *Landtek WM-106 Whiteness Meter*. Prior to analysis, the instrument was calibrated using the certified white reference plate supplied by the manufacturer. Samples were positioned on the measurement aperture and analyzed under a 45°/0° optical geometry with a 457 nm LED illumination source. Whiteness was quantified according to the Blue Light Whiteness index (WB = R457). The resulting values were recorded within the instrument's specified operational range (0-120).

2.2.16. Water activity

Water activity of the dried ESN hydrolysate samples was measured using a Water Activity Meter (Novasina LabPARTNER-aw). Approximately ±1.0 g of homogenized room-temperature powder was placed evenly in a sample cup and measured until a stable reading was obtained (±5-10 minutes).

2.2.17. Statistical analysis

A completely randomized design (CRD) was implemented for entire studies. One-way analysis of variance (ANOVA) was used and Tukey test was carried out to analyze the significant differences among samples at a level of ($p<0,05$) using SPSS version 27.0.1.0.

3. Results and Discussion

3.1. Yield

The hydrolysis yields of ESN samples exhibited significant variation across material grades, as presented in Table 1. The highest yield was obtained for hESN-C (62.13%), whereas the lowest was recorded for hESN-CP (28%). The quantitative results revealed substantial differences in yield, demonstrating that extraction efficiency is governed by the synergistic interaction between raw material purity and the UAEH process.

Higher glycoprotein content in cleaned material (hESN-C) facilitated enhanced enzyme accessibility and substrate interaction, thereby maximizing peptide bond cleavage. These results are consistent with protein extraction optimization reported by Noor et al. (2022) [24]. Conversely, the presence of non-protein impurities such as feathers, dirt, and residual contaminants in hESN-D and hESN-CP increased steric hindrance and reduced the effectiveness of enzymatic penetration [14].

Table 1. %Yield of ESN hydrolysate

Sample	%Yield
hESN-C	62.13%
hESN-D	56.62%
hESN-CP	28.00%

Although hESN-CP produced lower yields relative to hESN-C, it demonstrated effective utilization of co-product waste. This was evidenced by the preservation of characteristic glycoprotein functional groups in FTIR spectra, detectable Amide I and II peaks without excessive structural degradation, and retention of bioactive components, including sialic acid. The application of UAEH provides a sustainable pathway for processing ESN co-product waste from the swiftlet farming industry into high-value materials that support circular bioeconomy practices.

UAEH methods enhance the liberation of bioactive components through ultrasonic cavitation, which disrupts the ESN matrix and improves enzyme penetration, thereby increasing extraction efficiency [14]. This improvement is reflected in the high yields of hESN-C and hESN-D, both exceeding 50% and consistent with the characteristics of high-quality ESN, which typically contain 59-61% protein, whereas lower-grade materials with <55% protein produce lower yields [24]. Because protein represents the main soluble fraction in UAEH, samples with lower protein content and more insoluble material, such as hESN-CP, yield smaller extractable fractions. Enzymatic hydrolysis further enhances extraction by converting glycoproteins into smaller glycopeptides [12,13], although its efficiency depends on pretreatment conditions that may affect protein structure [9]. The integrated UAEH approach confers synergistic advantages that collectively enhance the overall efficiency of hydrolysate production.

3.2. FTIR analysis

Fourier Transform Infrared (FTIR) spectroscopy was employed to characterize the functional groups of ESN hydrolysates produced using ultrasound-assisted enzymatic hydrolysis. Spectral measurements recorded in the wavenumber range of 4000-500 cm^{-1} in Fig. 4 show characteristic absorption bands associated with the glycoprotein structural components of ESN.

A broad absorption band centered at approximately 3270-3400 cm^{-1} was assigned to O–H and N–H stretching vibrations, confirming the presence of hydroxyl and amine functionalities characteristic of ESN glycoproteins. As observed in the figure, hESN-C and ESN-C exhibit deeper and broader bands in this region compared to ESN-CP and hESN-CP, which display relatively lower absorption, consistent with the lower

glycoprotein purity of the co-product fraction. The Amide I band was detected at 1630-1640 cm^{-1} as a distinct absorption band across all samples, indicative of C=O stretching vibrations correlated with peptide backbone conformations. The Amide II band at 1526-1540 cm^{-1} was attributed to N–H bending coupled with C–N stretching, confirming vibrational modes of the protein structure. All samples, including the co-product hESN-CP, displayed these characteristic bands, indicating that the peptide backbone remained present despite the higher impurity level. The lower peak intensity observed in hESN-CP and ESN-CP reflects reduced hydrogen bonding and partial structural disruption, consistent with their lower hydrolysis yield.

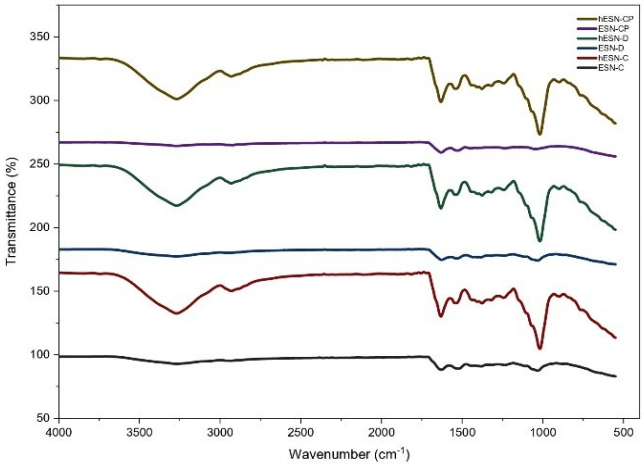

Fig. 4. FTIR spectra of ESN and hESN

The close similarity of spectral profiles obtained from hESN-C and hESN-D suggests that UAEH-mediated hydrolysis effectively cleaved peptide linkages while preserving the integrity of the glycoprotein backbone. The ESN glycoprotein has two structurally distinct components. The polypeptide backbone (subject to cleavage by bromelain) and the glycan chains (O- and N-linked oligosaccharides, including sialic acid) attached to the protein core. Bromelain is a cysteine protease with specificity for peptide bonds flanked by hydrophobic and bulky residues; it does not possess glycosidase activity and therefore cannot cleave glycosidic linkages. Consequently, even when peptide bonds are extensively hydrolyzed (generating a DH of 37.95%), the glycan moieties remain covalently attached to the resulting glycopeptide fragments, producing bioactive glycopeptides that retain their carbohydrate functional groups.

In the 1700-1500 cm^{-1} region, sharper peaks in UAEH-processed and freeze-dried hESN samples, most prominently observed in hESN-C (red), primarily arise from C=O stretching vibrations associated with carboxylate or amide groups. Compared to raw material, a slight band shift and intensity enhancement reflect alterations in the chemical environment induced by UAEH and freeze-drying processes. The characteristic Amide I band (1630-1640 cm^{-1}) and Amide II band (1530-1540 cm^{-1}) indicate the primary protein structure of ESN; in raw materials (ESN-C and ESN-D), these bands appear broader and less defined, whereas post-extraction they become sharper and more intense, suggesting enhanced structural regularity and protein purity [25,26].

Peaks in the 1200-1000 cm^{-1} region, associated with C–O and C–N stretching vibrations, indicate the presence of carbohydrate moieties characteristic of glycoproteins in ESN raw materials [9]. The raw material spectrum exhibits relatively broad bands, reflecting complex glycosidic linkages inherent to native glycoproteins. Following UAEH treatment, bands in this region become more resolved and distinctly separated, most notably in hESN-C, indicating structural reorganization of the glycoprotein carbohydrate domain into shorter glycopeptide fragments while the glycosidic linkages themselves remain intact. This band sharpening reflects increased mobility and reduced steric constraints of glycan chains when liberated from the high-molecular-weight glycoprotein scaffold into smaller glycopeptides [27,28].

These observations are consistent with previous reports by Ling et al. (2020) and Wang et al. (2024), which also demonstrated structural preservation of glycan moieties in ESN glycoproteins under enzymatic hydrolysis conditions. The persistence of stable amide and carbohydrate bands in the FTIR spectra of all UAEH-processed samples, together with confirmed sialic acid retention by HPLC, collectively demonstrates that UAEH achieves selective peptide bond hydrolysis without compromising glycosidic linkage integrity [14,29]. The persistence of stable amide and carbohydrate bands reinforces the structural robustness of ESN glycopeptide products under UAEH conditions, highlighting their potential for advanced applications such as nutraceuticals, functional foods, bioactive supplements, and cosmeceutical formulations, while simultaneously offering a value-added approach to mitigate ESN co-product waste and support circular bioeconomy practices.

3.3. Degree of hydrolysis

The degree of hydrolysis (DH) of UAEH-processed ESN hydrolysates exhibited a clear decreasing trend from cleaned to co-product fractions, as presented in Table 2. The highest DH was recorded in hESN-C at 37.95%, followed by hESN-D at 17.24%, with the lowest value observed in hESN-CP at 9.57%. This rank order (hESN-C > hESN-D > hESN-CP) reflects the progressive decrease in substrate purity and glycoprotein accessibility across the three ESN grades and is consistent with the electrochemical behavior observed in the cyclic voltammogram presented in Fig. 5.

Table 2. %Hydrolysis increase of ESN hydrolysate

Sample	%Hydrolysis Increase
hESN-C	37.95%
hESN-D	17.24%
hESN-CP	9.57%

As illustrated in Fig. 5, the cyclic voltammetric profiles of the three hydrolysates display overlapping sigmoid-shaped curves spanning the potential window from -2.0 V to +2.0 V relative to Ag/AgCl. In the cathodic sweep region (approximately -2.0 to -1.0 V), hESN-C exhibits the most pronounced reduction peak amplitude, consistent with its highest free amino group population liberated during

hydrolysis, directly reflecting a DH of 37.95%. The hESN-D displays an intermediate reduction response in this potential window, corresponding to its moderate DH of 17.24%, while hESN-CP exhibits the smallest cathodic peak amplitude, corroborating its lowest DH value of 9.57%. The visible separation between the three curves within the -2.0 to -1.0 V potential window provides direct electrochemical evidence of the quantitative DH differences reported in Table 2. In contrast, the convergence of the hESN-D and hESN-CP voltammetric curves in the anodic sweep region (0 to +2.0 V) further reflects the reduced electroactive free amino group populations in these lower-purity fractions, consistent with their comparatively limited peptide bond cleavage during UAEH. The overall voltammetric profile is characteristic of quasi-reversible redox behavior associated with the oxidation and reduction of free amine-containing peptide species, as reported for protein hydrolysate characterization using adsorptive stripping voltammetry [24].

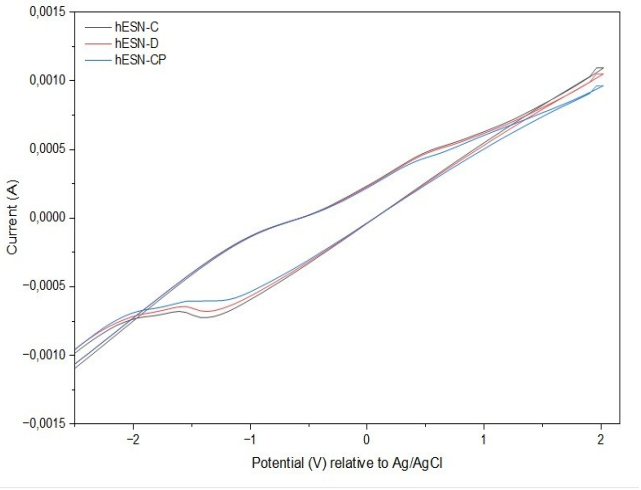

Fig. 5. Degree of hydrolisis of hESN

The DH values determined via adsorptive stripping voltammetry (VA Computrace 797) are corroborated by multiple independent physicochemical parameters measured in this study. The rank order of DH (hESN-C > hESN-D > hESN-CP) is precisely consistent with the rank order of soluble protein content (1.246 > 1.073 > 0.844 µg/µL), particle size reduction (smaller nanoparticles in hESN-CP corresponding to greater structural disruption), and DPPH radical scavenging activity (16.12% > 15.97% > 10.70%), providing robust internal cross-validation of the voltammetric DH measurements and confirming the internal coherence of the dataset.

The systematic differences in DH across the three grades are primarily attributable to variations in substrate purity and protein accessibility. The hESN-C, derived from thoroughly cleaned swiftlet nests, contains a higher proportion of intact glycoproteins with minimal non-protein impurities, enabling bromelain to more efficiently access and hydrolyze peptide bonds during UAEH processing. The absence of physical barriers in the high-purity substrate facilitates the formation of stable enzyme–substrate complexes, thereby maximizing cleavage of glycoprotein chains and yielding the highest DH of 37.95%. These findings are consistent with the report by Ling et al. (2020), who demonstrated that cleaned ESN substrates yield higher hydrolysis efficiency without degradation of the primary glycoprotein structure [14], and with the general principle that high-purity protein substrates enhance bromelain catalytic performance under optimized UAEH conditions [24].

In contrast, hESN-D and hESN-CP contain progressively higher levels of residual impurities, including dirt, feathers, and insoluble non-protein matrix components, that physically obstruct enzyme–substrate interactions and reduce the accessible peptide bond surface area, resulting in substantially lower DH values of 17.24% and 9.57%, respectively. The structural complexity of co-product matrices imposes additional steric constraints on bromelain activity, limiting the overall efficiency of peptide bond cleavage. The convergence of hESN-D and hESN-CP voltammetric curves observed in Fig. 5 in the anodic region further reflects the electrochemically diminished free amino group populations in these fractions, consistent with their reduced degree of hydrolysis. Nonetheless, even at a DH of 9.57%, hESN-CP demonstrated measurable bioactive potential, including detectable sialic acid retention, improved soluble protein content, and DPPH inhibition of 10.70%, indicating that UAEH processing remains effective in generating functionally relevant glycopeptide fractions even from lower-purity co-product substrates.

The enhancement in DH observed across all three grades relative to non-hydrolyzed controls is mechanistically attributable to the synergistic dual action of UAEH. Ultrasonic cavitation physically disrupts the intact ESN structural matrix through intense shear forces and acoustic microstreaming, reducing particle size, increasing enzyme-accessible surface area, and facilitating bromelain penetration into the glycoprotein substrate. This physical pretreatment accelerates glycopeptide liberation and augments overall enzymatic efficiency, as previously established for ultrasound-assisted enzymatic processing of high-molecular-weight glycoprotein substrates [17,2]. The combined effect of substrate disruption and enzymatic cleavage explains why the DH values obtained in the present study, particularly for hESN-C (37.95%), are substantially higher than those typically reported for conventional non-assisted enzymatic hydrolysis of EBN materials. The process parameters applied in this study, including optimized sonication power, pH, and enzyme concentration, were therefore critical determinants of the DH outcome across all three ESN grades.

3.4. Profiling amino acid

Table 3. presents the amino acid profiles of hESN-C, hESN-D, and hESN-CP. Amino acid analysis reveals that each hESN type contains 18 amino acids. The results indicate that ESN hydrolysates contain a complete profile of essential amino acids (EAAs), with varying composition depending on the raw material type.

Table 3. Profiling amino acid

Parameters	Unit	hESN-C	hESN-D	hESN-CP	Limit of Detection	Method
L-Alanine	mg/kg	11193.88	6954.49	2581.34	-	11-6-4/MU (UPLC-PDA)
L-Arginine	mg/kg	35852.75	16192.20	3179.33	-	11-6-4/MU (UPLC-PDA)
L-Aspartic Acid	mg/kg	30186.27	21176.11	6383.82	-	11-6-4/MU (UPLC-PDA)
Glycine	mg/kg	16080.39	8043.85	2473.69	-	11-6-4/MU (UPLC-PDA)
L-Glutamic Acid	mg/kg	26080.81	19638.69	6244.67	-	11-6-4/MU (UPLC-PDA)
L-Histidine	mg/kg	15776.32	9079.57	1747.11	-	11-6-4/MU (UPLC-PDA)
L-Isoleucine	mg/kg	13463.19	9054.15	2557.30	-	11-6-4/MU (UPLC-PDA)
L-Cysteine	mg/kg	15211.08	18879.34	5042.39	-	11-7-2/MU (LC-MS/MS)
L-Leucine	mg/kg	28650.07	17253.52	4681.34	-	11-6-4/MU (UPLC-PDA)
L-Lysine	mg/kg	13206.46	9334.14	2226.23	-	11-6-4/MU (UPLC-PDA)
L-Methionine	mg/kg	1278.34	881.11	280.57	-	11-7-2/MU (LC-MS/MS)
L-Tryptophan	mg/kg	3262.62	2906.47	969.53	-	11-6-5/MU (HPLC-PDA)
L-Valine	mg/kg	36507.33	18151.61	4424.76	-	11-6-4/MU (UPLC-PDA)
L-Phenylalanine	mg/kg	28465.08	17170.00	3548.69	-	11-6-4/MU (UPLC-PDA)
L-Proline	mg/kg	37083.32	18890.46	4614.71	-	11-6-4/MU (UPLC-PDA)
L-Serine	mg/kg	37635.48	12503.89	3009.81	-	11-6-4/MU (UPLC-PDA)
L-Threonine	mg/kg	29285.56	16850.47	4088.93	-	11-6-4/MU (UPLC-PDA)
L-Tyrosine	mg/kg	23805.56	12554.61	3012.05	-	11-6-4/MU (UPLC-PDA)

In hESN-C, the essential amino acids with the highest concentrations are L-valine (36507.33 mg/kg), L-leucine (28650.07 mg/kg), L-threonine (29285.56 mg/kg), and L-phenylalanine (28465.08 mg/kg). In hESN-D, the highest-concentration essential amino acids are L-valine (18151.61 mg/kg), L-leucine (17253.52 mg/kg), L-phenylalanine (17170.00 mg/kg), and L-threonine (16850.47 mg/kg). Meanwhile, in hESN-CP, the essential amino acids with the highest concentrations are L-leucine (4681.34 mg/kg), L-valine (4424.76 mg/kg), L-threonine (4088.93 mg/kg), and L-phenylalanine (3548.69 mg/kg).

These findings align with the research by Chantakun and Benjakul (2022), which reported that protein hydrolysate from ESN co-product contained leucine, threonine, lysine, and valine as the primary essential amino acids, with respective percentages of 4.28%, 3.53%, 3.30%, and 3.08% of the total sample [7]. The similar distribution pattern of essential amino acids indicates that the enzymatic hydrolysis process can retain the intrinsic nutritional characteristics of ESN, regardless of the raw material source.

A comparison of essential amino acid concentrations among the three samples shows a consistent decrease from hESN-C to hESN-D, and further to hESN-CP. This phenomenon can be explained by several factors. The hESN-C, derived from clean nests, has a higher content of pure salivary protein, while hESN-D contains contaminants such as feathers and eggshells that dilute the protein concentration. Chantakun and Benjakul (2020) stated that ESN comprises 85-97% saliva and 3-15% feathers, and during the cleaning process, the co-product consisting of broken nests, feathers, and eggshells accounts for approximately 30% of the total ESN [7]. This explains why hESN-CP has significantly lower amino acid content, as the co-product contains a higher proportion of non-protein materials. Nonetheless, hESN-CP products can serve as an alternative source of essential amino acids beneficial for the body, supporting their valorization as functional ingredients in nutraceutical and food supplement applications.

3.5. Profiling fatty acid

Table 4 revealed that the ESN hydrolysates have varying fatty acid compositions across samples, both in terms of type and concentration. Based on the test results, several saturated and unsaturated fatty acids were detected at different concentrations in each sample. This variation reflects differences in lipid characteristics formed or retained during the hydrolysis process, illustrating the dynamics of changes in the fat fraction of the final product.

The identified saturated fatty acids included myristic acid (C14:0), palmitic acid (C16:0), and stearic acid (C18:0). Myristic acid was detected only in hESN-CP at a relatively low level, indicating selective distribution across sample types. In contrast, palmitic and stearic acids were detected more consistently, with the highest concentrations found in the hESN-CP sample. This suggests that these long-chain saturated fatty acids are the main lipid components in ESN hydrolysates and possess greater stability compared to other saturated fatty acids.

In addition to saturated fats, hESN-CP also contained unsaturated fat at 0.19%. Oleic acid (C18:1, omega-9) was the main component, accounting for 0.1491%. Linoleic acid (C18:2, omega-6) was also detected in this sample at 0.0428%, which aligns with a polyunsaturated fat value of 0.04%. The presence of oleic and linoleic acids indicates that hESN-CP

contains nutritionally valuable unsaturated fatty acids. Unsaturated fatty acids are lipid components known to enhance memory, learning, and cognitive function, while also supporting nerve cell health and brain structure [30,31]. Oleic acid, a monounsaturated omega-9 fatty acid, plays a crucial role in nerve cell formation and is fundamental in preventing cardiovascular diseases [32]. The presence of oleic acid in ESN hydrolysates has also been reported as one of the dominant metabolites based on GC-MS analysis, reinforcing the role of ESN lipids as bioactive compounds supporting health benefits. Linoleic acid, an omega-6 polyunsaturated fatty acid, is considered essential for healthy human skin growth. Consequently, ESN serves as a good source of omega fatty acids, and its consumption may offer several nutritional benefits for humans [32].

Table 4. Profiling fatty acid

Parameters	Unit	hESN-C	hESN-D	hESN-CP	Limit of Detection	Method
C 14:0 (Myristic Acid)	%	-	-	0.0276	-	11-4-1/MU (GC)
C 16:0 (Palmitic Acid)	%	-	0.0478	0.2263	-	11-4-1/MU (GC)
C 18:0 (Stearic Acid	%	-	0.0149	0.0741	-	11-4-1/MU (GC)
Saturated Fat	%	0.15	0.06	0.33	-	11-4-1/MU (GC)
Unsaturated Fat	%	0.59	0.05	0.19	-	11-4-1/MU (GC)
Polyunsaturated Fats	%	-	-	0.04	-	11-4-1/MU (GC)
Monounsaturated Fat	%	0.59	0.05	0.15	-	11-4-1/MU (GC)
Omega 6 Fatty Acids	mg/100g	-	-	42.8	-	11-4-1/MU (GC)
Omega 9 Fatty Acids	mg/100g	192.1	47.3	149.1	-	11-4-1/MU (GC)
Oleic Acid	%	0.1921	0.0473	0.1491	-	11-4-1/MU (GC)
Linoleic Acid	%	-	-	0.0428	-	11-4-1/MU (GC)
C 13:0 (Tridecanoic Acid)	%	0.1470	-	-	-	11-4-1/MU (GC)
C 16:1 (Palmitoleic Acid)	%	0.1739	-	-	-	11-4-1/MU (GC)

In comparison, the hESN-C sample displayed different characteristics, dominated by monounsaturated fatty acids. The total unsaturated fat in this sample was recorded at 0.59%, entirely attributed to oleic acid at a concentration of 0.1921%. Furthermore, hESN-C also contained tridecanoic acid (C13:0) at 0.1470% and palmitoleic acid (C16:1) at 0.1739%, which were not detected in hESN-CP. However, hESN-C did not show the presence of polyunsaturated fatty acids, resulting in an overall lower diversity of fatty acids compared to hESN-CP.

Meanwhile, the hESN-D sample exhibited the simplest fatty acid profile with relatively low total concentrations. The total saturated fat in this sample was 0.06%, primarily contributed by palmitic acid at 0.0478% and stearic acid at 0.0149%. Oleic acid was detected in a limited amount of 0.0473%, consistent with a monounsaturated fat value of 0.05%. The absence of detectable polyunsaturated fatty acids in hESN-D indicates that the PUFA fraction is present at extremely low levels or falls below the detection limit.

3.6. Sialic acid

The qualitative presence of sialic acid in all ESN hydrolysate samples was confirmed through HPLC chromatographic analysis, as presented in Fig. 6. Characteristic peaks appearing within the retention time window of 6.2-6.8 min were consistently detected across all six chromatograms, providing qualitative evidence of sialic acid retention following UAEH processing and freeze-drying.

For the ESN-C grade, the raw material chromatogram in Fig. 6(a) displays a dominant, high-intensity peak at 6.202 min (~240 mAU), accompanied by minor satellite peaks at 5.328 min and 7.109 min, and a late-eluting peak at 23.230 min attributable to residual matrix components. The elevated peak intensity in the raw ESN-C chromatogram reflects the intact, high-molecular-weight glycoprotein matrix prior to hydrolysis. Following UAEH processing, the hESN-C chromatogram in Fig. 6(b) exhibits a well-resolved cluster of peaks at 6.323-6.482 min, accompanied by a secondary peak at 10.100 min. The shift toward a multi-peak cluster with improved resolution in hESN-C relative to the single dominant peak in ESN-C is consistent with glycopeptide fragmentation during hydrolysis, which liberates sialic acid-bearing glycopeptides of varying chain lengths and increases their chromatographic resolution.

For the ESN-D grade, the raw material chromatogram in Fig. 6(c) presents a prominent peak at 6.419 min (~190 mAU) with an adjacent shoulder at 6.221 min, alongside minor peaks at 6.586 min and 10.010 min, and an early-eluting peak at 0.499 min attributed to solvent or buffer matrix components. The multi-peak profile observed even in the raw ESN-D material suggests a more heterogeneous glycoprotein composition relative to ESN-C. The corresponding hESN-D chromatogram in Fig. 6(d) exhibits a sharp, well-defined dominant peak at 6.417 min, with satellite peaks at 6.029 min, 6.295 min, 7.984 min, and 9.993 min. The sharpened dominant peak and preserved retention time in hESN-D relative to its raw material indicate that UAEH treatment maintained sialic acid structural integrity while generating additional resolved glycopeptide fractions, consistent with partial hydrolysis of the surrounding peptide matrix without disruption of the glycan moiety itself.

For the co-product fraction, the raw ESN-CP chromatogram

in Fig. 6(e) displays a pronounced peak at 6.511 min (~270 mAU), the highest baseline intensity among all raw material chromatograms, accompanied by a cluster of overlapping minor peaks between 6.245 min and 6.641 min, reflecting the more heterogeneous glycoprotein matrix characteristic of co-product material with greater structural complexity. Following UAEH processing, the hESN-CP chromatogram in Fig. 6(f) presents a well-defined dominant peak at 6.684 min with a resolved shoulder at 6.823 min and additional minor peaks at 6.427 min, 7.254 min, and 10.060 min. The emergence of a more resolved peak pattern in hESN-CP post-hydrolysis, despite the inherently heterogeneous composition of the co-product fraction, confirms sialic acid retention and partial liberation of glycopeptide-bound sialic acid structures following UAEH treatment.

The retention times observed across all six chromatograms (6.2-6.8 min) are in close agreement with reference values reported by Mahaq et al. (2024) at 6.40 min and Wang et al. (2024) at approximately 7 min, supporting the chromatographic identity of the detected peaks as sialic acid [29,33,34]. It is important to note that the HPLC analysis in this study was conducted as a qualitative screen to verify sialic acid retention following UAEH processing and freeze-drying; absolute quantification (expressed as mg/g or µmol/g) was not performed. The consistent detection of sialic acid across all sample grades, hESN-C, hESN-D, and hESN-CP, confirms that neither UAEH processing nor freeze-drying eliminated this characteristic glycan, which is mechanistically consistent with bromelain's protease-exclusive specificity and its inability to cleave glycosidic bonds.

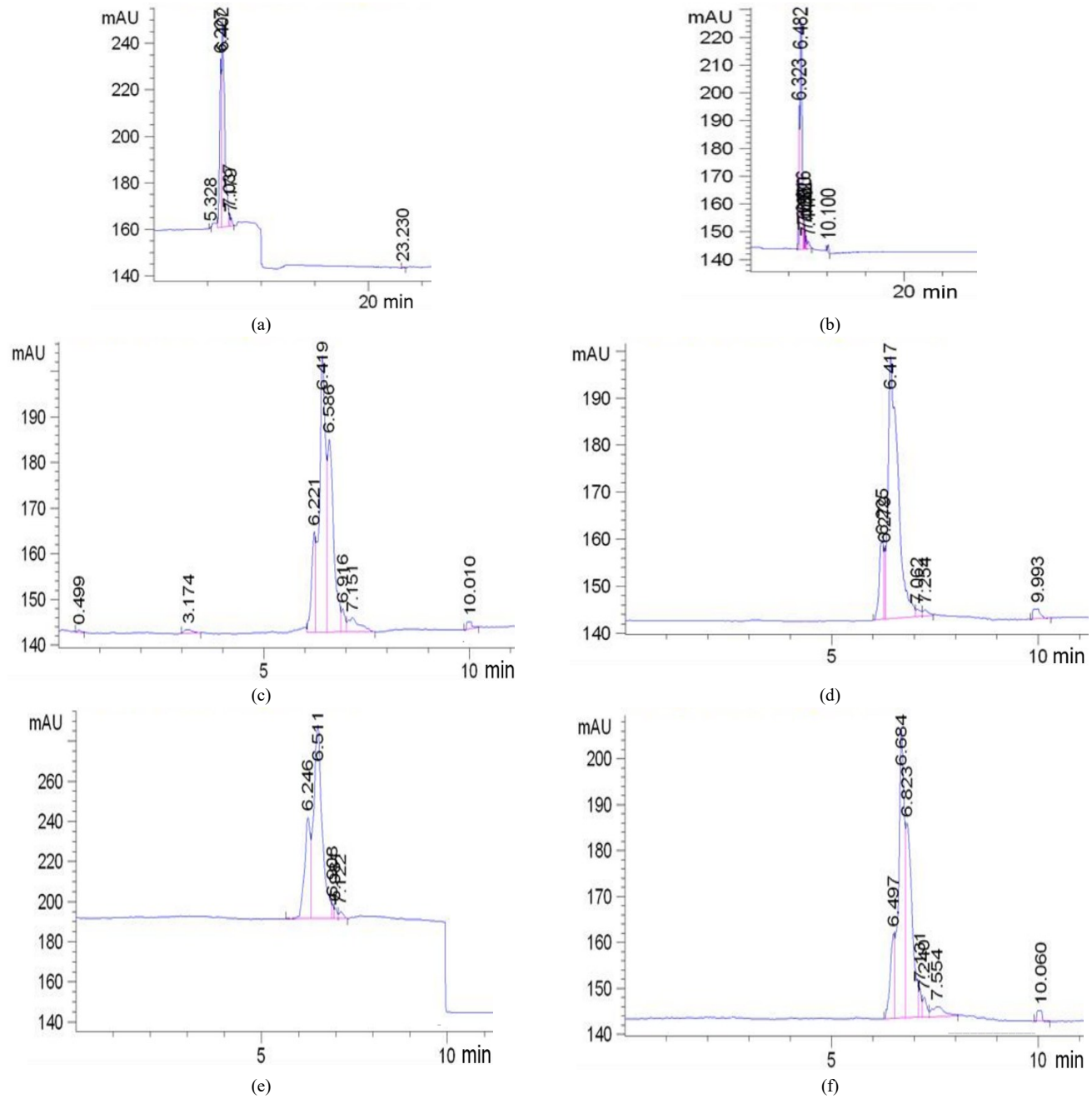

Fig. 6. HPLC chromatogram of (a) raw ESN C, (b) hESN C, (c) raw ESN D, (d) hESN D, (e) raw ESN CP, (f) hESN CP

The detection of sialic acid in all samples is directly corroborated by the FTIR spectroscopic analysis presented in Fig. 4, which confirmed the preservation of glycoprotein structural integrity following UAEH treatment. The characteristic absorption bands at 3270-3272 cm^{-1} (O–H and N–H stretching), Amide I (1630-1631 cm^{-1}), and Amide II (1526-1537 cm^{-1}) confirm that the glycoprotein backbone remained intact despite enzymatic hydrolysis. Furthermore, absorption peaks in the 1200-1000 cm^{-1} region, associated with C–O and C–N stretching vibrations, indicate the presence of carbohydrate moieties characteristic of glycoproteins, including sialic acid residues covalently linked to the protein backbone.

The glycoprotein identity of ESN and the structural basis for sialic acid retention are further supported by the amino acid profiling data in Table 3, which revealed a predominance of hydroxyl-containing hydrophilic amino acids across all hydrolysate samples. In particular, L-serine (37635.48 mg/kg in hESN-C), L-threonine (29285.56 mg/kg in hESN-C), and L-proline (37083.32 mg/kg in hESN-C) are commonly associated with mucin-type glycoproteins in which serine and threonine residues serve as O-glycosylation sites for oligosaccharide chains containing sialic acid [5,7]. The preservation of these amino acids in the hydrolysate fraction provides indirect structural evidence that sialic acid-bearing glycan chains remained attached to the peptide backbone following UAEH treatment.

The qualitative retention of sialic acid across all UAEH-processed hydrolysates, as confirmed by HPLC chromatographic peaks at 6.2-6.8 min in Fig. 6, is of significant bioactive relevance. N-acetylneuraminic acid (Neu5Ac), the predominant sialic acid species in ESN, has been reported in the literature to support cognitive function and brain ganglioside synthesis, as demonstrated in animal models by Loh et al. (2022) and Mahaq et al. (2024) [6,33,34]. Sialic acid-bearing glycopeptides in ESN have also been associated with immunomodulatory effects mediated through interaction with Siglec receptors on immune cells [4]. It must be emphasized, however, that the sialic acid data in this study are qualitative in nature, confirming presence but not absolute concentration, and therefore claims regarding bioactive potential are referenced from the established literature rather than asserted as direct outcomes of the present study. Quantitative sialic acid determination using validated methods such as the thiobarbituric acid (TBA) colorimetric assay or fluorometric HPLC with 1,2-diamino-4,5-methylenedioxybenzene (DMB) derivatization is recommended in future studies to enable inter-sample quantitative comparison and dose-response characterization for nutraceutical and functional food applications.

3.7. Soluble protein

Protein solubility is a thermodynamic parameter that describes the capacity of proteins to disperse homogeneously in aqueous media under defined equilibrium conditions. This parameter is primarily governed by the surface distribution of hydrophobic and hydrophilic amino acid residues and the nature of protein-water molecular interactions. Proteins with greater surface exposure of hydrophilic groups generally exhibit superior solubility, attributable to more stable hydrogen bonding and electrostatic interactions with surrounding water molecules. Previous investigations have reported that EBN prior to hydrolysis contains a relatively high crude protein content of approximately 58.63%; however, despite this substantial protein content, the solubility of native EBN proteins remains inherently limited due to their large molecular size and complex glycoprotein architecture. Following enzymatic hydrolysis, EBN proteins undergo a significant increase in aqueous solubility. EBN hydrolysates produced through combined boiling and papain hydrolysis have been reported to achieve soluble protein levels of up to ±45.96% at a degree of hydrolysis of 11.19%, indicating extensive cleavage of polypeptide chains into smaller and more dispersible peptide fractions [9].

Table 5. Soluble protein of hESN

Samples	Soluble Protein (ug/uL)
ESN-C	1.202
ESN-D	0.675
ESN-CP	0.022
hESN-C	1.246
hESN-D	1.073
hESN-CP	0.844

As presented in Table 5, the soluble protein content of non-hydrolyzed raw materials was comparatively low across all grades. ESN-C and ESN-D recorded soluble protein values of 1.202 μg/μL and 0.675 μg/μL, respectively, while ESN-CP exhibited a markedly lower value of 0.022 μg/μL. In this study, these non-hydrolyzed raw materials served as baseline controls against which the effect of UAEH treatment was evaluated, enabling direct quantification of the improvement attributable to the combined ultrasound-enzymatic process. The low solubility observed in these raw materials reflects the predominance of proteins in the form of intact, high-molecular-weight glycoproteins characterized by strong hydrophobic interactions and limited surface accessibility of hydrophilic residues, which restricts their capacity to disperse in aqueous media. These observations are consistent with previous reports indicating that EBN proteins prior to hydrolysis typically display poor aqueous solubility due to their high molecular weight and the absence of significant peptide fragmentation [35,36].

Following UAEH processing and subsequent freeze-drying, the soluble protein content increased significantly in all sample grades, as shown in Table 5. The hESN-C, hESN-D, and hESN-CP recorded soluble protein values of 1.246 μg/μL, 1.073 μg/μL, and 0.844 μg/μL, respectively. The most substantial improvement was observed in hESN-CP, which increased from 0.022 μg/μL to 0.844 μg/μL, representing a 38-fold increase relative to the unhydrolyzed ESN-CP baseline. Similarly, hESN-D demonstrated a marked improvement from 0.675 μg/μL to 1.073 μg/μL, while hESN-C showed a moderate but consistent increase from 1.202 μg/μL to 1.246 μg/μL. These results collectively confirm that enzymatic hydrolysis plays a critical role in enhancing protein solubility by fragmenting

polypeptide chains into shorter peptide units, thereby increasing the surface exposure of hydrophilic residues and facilitating more favorable interactions with water molecules [24]. The magnitude of improvement across all three grades demonstrates the effectiveness of UAEH in transforming ESN co-product materials into functionally enhanced hydrolysates with superior bioavailability characteristics.

The enhanced solubility observed in UAEH-treated samples is strongly supported by the amino acid profiling results presented in Table 3, which revealed a predominance of hydrophilic amino acids that directly contribute to aqueous protein dispersion. In hESN-C, the highest amino acid concentrations were recorded for L-serine (37635.48 mg/kg), L-proline (37083.32 mg/kg), L-valine (36507.33 mg/kg), and L-threonine (29285.56 mg/kg), consistent with its superior soluble protein content of 1.246 μg/μL. Serine and threonine are hydroxyl-containing amino acids that form strong hydrogen bonds with water molecules, while proline, despite its hydrophobic character in isolation, contributes to peptide chain flexibility and enhanced exposure of hydrophilic residues within glycopeptide structures [7]. In hESN-D, elevated concentrations of L-valine (18151.61 mg/kg), L-leucine (17253.52 mg/kg), L-phenylalanine (17170.00 mg/kg), and L-threonine (16850.47 mg/kg) support its intermediate soluble protein value of 1.073 μg/μL. Even in hESN-CP, which exhibited the lowest total amino acid content, the presence of L-leucine (4681.34 mg/kg), L-valine (4424.76 mg/kg), and L-threonine (4088.93 mg/kg) contributed to a substantial post-hydrolysis solubility improvement, with soluble protein increasing from 0.022 μg/μL to 0.844 μg/μL. The proportional relationship between hydrophilic amino acid content and soluble protein levels across all grades confirms that amino acid composition is a primary determinant of protein solubility in ESN hydrolysates.

The mechanistic basis by which UAEH enhances protein solubility can be understood through two complementary processes. Enzymatic hydrolysis cleaves peptide bonds within intact glycoprotein chains, generating shorter peptide fragments with higher surface area to volume ratios and greater exposure of previously buried hydrophilic residues. Ultrasonic cavitation physically disrupts hydrophobic protein aggregates through intense shear forces and localised pressure gradients, reducing particle size and further increasing the accessible hydrophilic surface area [24]. The combined action of these mechanisms explains the consistent solubility enhancement observed across all three hydrolysate grades, hESN-C (1.246 μg/μL), hESN-D (1.073 μg/μL), and hESN-CP (0.844 μg/μL), relative to their respective unhydrolysed controls, ESN-C (1.202 μg/μL), ESN-D (0.675 μg/μL), and ESN-CP (0.022 μg/μL). The detection of a complete essential amino acid profile across all hydrolysate samples, including both hydrophilic (threonine and lysine) and hydrophobic (leucine, valine, isoleucine, and phenylalanine) residues, confirms that the UAEH process preserves nutritional completeness while concurrently optimising the physicochemical properties of the hydrolysates.

The effectiveness of ultrasonication in enhancing enzymatic efficiency is further attributed to its ability to modify protein tertiary and quaternary structure through cavitation-induced unfolding, thereby increasing the accessibility of peptide bonds to bromelain activity and facilitating the liberation of amino acids from complex glycoprotein matrices. The degree of solubility enhancement is also influenced by process parameters including pH, sonication time, ultrasonic power density, and substrate concentration, all of which were systematically optimized in the present study. When these parameters are properly controlled, UAEH can maximize solubility improvement while maintaining the structural integrity of bioactive glycopeptides and preserving the essential amino acid profile. The retention of all 18 amino acids identified in the profiling analysis, including the nine essential amino acids required for human nutrition, confirms that the UAEH process does not induce significant amino acid degradation or loss. This preservation of amino acid integrity, combined with the substantially enhanced soluble protein contents recorded in Table 5, renders the resultant hydrolysates particularly suitable for incorporation into functional beverages, nutritional supplements, and bioactive formulations where both nutritional value and functional performance constitute critical quality determinants.

3.8. Viscosity

Based on the results presented in Table 6, sample hESN-C exhibited the highest viscosity of 2.56±0.04 mPa·s, followed by hESN-D at 2.50±0.03 mPa·s. These values indicate that the glycoprotein structures in both samples remained relatively intact, thereby allowing the solutions to retain their viscosity. In contrast, sample hESN-CP displayed a lower viscosity of 1.90±0.04 mPa·s, suggesting that the UAEH treatment applied to this sample induced more extensive protein structural breakdown compared to the other two samples.

Different letters denote the significant difference ($p < 0.05$)

Furthermore, bromelain enzyme contains a closely related mixture of proteolytic enzymes with broad substrate specificity, making it highly effective in hydrolyzing large glycoproteins into smaller molecules, thereby enhancing the efficiency of the hydrolysis process [37]. The cleavage of proteins into small fragments consequently leads to a reduction in solution viscosity, as observed in hESN-CP. This observation is consistent with Tai et al. (2020), who reported that bromelain is capable of breaking protein bonds effectively [17].

Table 6. Viscosity of hESN

Samples	Viscosity (mPa.s)
ESN-C	2.17±0.11a
ESN-D	1.87±0.04b
ESN-CP	1.84±0.03b
hESN-C	2.56±0.04c
hESN-D	2.50±0.03c
hESN-CP	1.90±0.04b

The decrease in viscosity observed in hESN-CP can be attributed to alterations in the physicochemical properties of the proteins. The viscosity of a protein solution is strongly influenced by molecular size, protein folding, degree of

aggregation, and intermolecular interactions such as disulfide bonds and electrostatic interactions. A large and complex protein structure typically yields a more viscous solution. Conversely, when proteins are broken down into smaller fragments, the number of intermolecular interactions diminishes, resulting in a thinner solution [38]. This condition is precisely what was observed in the hESN-CP sample, where extensive enzymatic hydrolysis resulted in lower viscosity values while potentially improving bioavailability and functional properties for application in liquid nutritional products.

3.9. Antioxidant activities of ESN hydrolysates

The antioxidant activity of ESN hydrolysate samples was evaluated by determining the percentage of DPPH radical inhibition, a widely employed in vitro method for assessing the hydrogen atom and electron transfer capacity of bioactive peptides and glycopeptides.

Table 7. Antioxidant activities of hESN

Samples	%Inhibition
ESN-C	9.29
ESN-D	8.03
ESN-CP	2.18
hESN-C	16.12
hESN-D	15.97
hESN-CP	10.70

As presented in Table 7, the DPPH radical scavenging activity of non-hydrolyzed raw materials was comparatively low, with ESN-C recording 9.29% inhibition, ESN-D recording 8.03%, and ESN-CP exhibiting the lowest value at 2.18% at a test concentration of 100 ppm. These baseline values reflect the inherent structural constraints of native ESN glycoproteins, in which aromatic and sulfur-containing residues responsible for radical quenching remain largely sequestered within intact polypeptide matrices and are therefore inaccessible for direct electron or hydrogen atom donation to DPPH radicals.

Following UAEH treatment, a statistically significant increase in antioxidant activity was observed across all sample grades ($p < 0.05$, Tukey test). As shown in Table 7, hESN-C exhibited the highest DPPH inhibition at 16.12%, followed by hESN-D at 15.97% and hESN-CP at 10.70%. The paired comparison between raw materials and their corresponding hydrolysates, ESN-C (9.29%) vs. hESN-C (16.12%), ESN-D (8.03%) vs. hESN-D (15.97%), and ESN-CP (2.18%) vs. hESN-CP (10.70%), directly demonstrates that the enhancement in radical scavenging capacity is attributable to the UAEH process itself rather than to intrinsic compositional differences between raw material grades. The consistent pattern of improvement across all three grades further substantiates this interpretation.

The mechanistic basis for the observed increase in DPPH scavenging activity following UAEH is the disruption of protein aggregates and glycoprotein matrix architecture through acoustic cavitation, which reduces particle size, increases molecular surface area, and liberates short bioactive peptides bearing aromatic residues (phenylalanine and tyrosine) and sulfur-containing amino acids, residues known to donate electrons or hydrogen atoms to DPPH radicals [44]. This interpretation is consistent with the amino acid profiling data presented in Table 3, wherein aromatic and sulfur-containing residues were detected across all hydrolysate fractions, supporting a mechanistic link between peptide liberation and enhanced radical scavenging capacity.

These findings are consistent with previous investigations on EBN-derived hydrolysates. Ling et al. (2020) reported DPPH inhibition values of 8.40-25.30% for EBN glycopeptide fractions [19], while Chantakun and Benjakul (2022) observed 15.20-22.40% inhibition for ultrasound-pretreated EBN co-product hydrolysates [7]. The values obtained in the present study (10.70-16.12% at 100 ppm) are therefore consistent with the reported range for ESN-specific glycopeptide hydrolysates and are not anomalously low within this substrate class. Furthermore, Chantakun and Benjakul (2022) confirmed that ESN subjected to hydrolysis exhibits higher free radical scavenging ability compared to untreated raw material [7], and Wen et al. (2020) demonstrated that ultrasonic assistance further increases DPPH activity relative to non-ultrasonicated controls [39], both of which corroborate the findings of the present study.

The DPPH inhibition values obtained in this study are acknowledged to be modest in absolute terms when compared to protein hydrolysates derived from other substrates, including fish collagen peptides (50-85%), whey hydrolysates (40-75%), and soy peptide fractions (30-60%) at equivalent concentrations. This difference is attributable to the distinct compositional identity of ESN as a glycoprotein-dominated substrate, in which the glycan architecture, including sialic acid residues and O- and N-linked oligosaccharides, constitutes a major structural fraction rather than a high-density pool of aromatic or sulfur-containing residues that typically drive elevated DPPH scavenging capacity. Accordingly, DPPH radical scavenging does not represent the primary bioactive signature of ESN hydrolysates, and the values obtained are consistent with those reported specifically for ESN-derived glycopeptide fractions in the peer-reviewed literature [7,14]. Inter-material comparisons must therefore be interpreted within the compositional context of the source substrate.

It must be acknowledged that the DPPH inhibition values recorded in this study (10.70-16.12% at 100 ppm) represent a preliminary, single-assay, in vitro screen and do not constitute direct evidence of antioxidant efficacy in biological systems. No cell-based, animal model, or clinical bioassays were conducted in the present study. Accordingly, interpretive claims are confined to the following evidence-supported statements. The UAEH statistically significantly increased DPPH radical scavenging activity relative to non-hydrolyzed controls across all ESN grades ($p < 0.05$, Tukey test); the improvement is mechanistically consistent with the liberation of short bioactive peptides bearing aromatic and sulfur-containing residues; and the values are within the range reported for ESN hydrolysates in the existing literature [7,14]. Broader functional food or nutraceutical applications remain aspirational directions warranting further validation through multi-assay antioxidant profiling (e.g., ABTS, FRAP, and

ORAC assays), cellular oxidative stress models, and ultimately in vivo studies before definitive health claims can be substantiated.

3.10. Atomic absorption spectrofortrometry (AAS)

According to the AAS analysis presented in Table 8, Hg, Cd, and Pb were detected in hESN-C, hESN-D, and hESN-CP at low concentrations with distinct distribution patterns among sample types. Mercury concentrations ranged from 0.0172 to 0.0236 mg/L, showing a gradual increase from hESN-C (0.0172 mg/L) to hESN-D (0.0193 mg/L) and hESN-CP (0.0236 mg/L). A similar trend was observed for cadmium, with concentrations increasing from 0.1194 mg/L in hESN-C to 0.1405 mg/L in hESN-D and 0.1444 mg/L in hESN-CP. Lead exhibited the most pronounced variability, with the highest level detected in hESN-CP (1.4 mg/L), followed by hESN-D (0.17 mg/L) and hESN-C (0.11 mg/L).

Table 8. Heavy metal concentrations in hESN determined by AAS

Heavy Metals	Concentration (mg/L)			China Standard (ppm)
	hESN-C	hESN-D	hESN-CP	
Hg	0.0172	0.0193	0.0236	0.05
Cd	0.1194	0.1405	0.1444	1.00
Pb	0.1100	0.1700	1.4000	2.00

Importantly, all measured heavy metal concentrations remained below the maximum permissible limits established by the China Standard (Hg ≤ 0.05 ppm, Cd ≤ 1 ppm, Pb ≤ 2 ppm), confirming the regulatory compliance and safety of all UAEH-processed hESN co-product hydrolysates. These findings further demonstrate that the UAEH process effectively preserved the inherent elemental characteristics of the raw materials without promoting heavy metal enrichment, while the subsequent freeze-drying step maintained product stability by producing a dehydrated hESN hydrolysate with minimal compositional alteration, an important consideration for both physicochemical integrity and bioactivity retention [11].

Quantification of Hg, Cd, and Pb was performed using external calibration based on linear regression of absorbance versus standard concentration in Fig. 7. The calibration curves for Hg, Cd, and Pb exhibited good linearity within the studied concentration ranges, as indicated by high coefficients of determination ($R^2 > 0.999$). The strong linear correlations confirm the suitability and reliability of the AAS method for accurate determination of these heavy metals in hESN samples.

The assessment of heavy metal safety in UAEH-processed ESN co-product hydrolysates refers to the tolerance limits specified in CAIQ-RZ-20052. As a major importing country, China has established comprehensive regulatory frameworks through CAIQ RZ-2015001 Bird's Nest Product Processing Enterprise Hygienic Technical Specifications and CAIQ-RZ-2015002 Bird's Nest Product Certification Implementation Rules, which govern hygiene control and product safety in ESN processing and international trade [40]. Adherence to these standards is critical for ensuring product acceptance in global markets and minimizing potential health risks associated with heavy metal exposure, particularly given the growing demand for ESN co-product-derived functional ingredients.

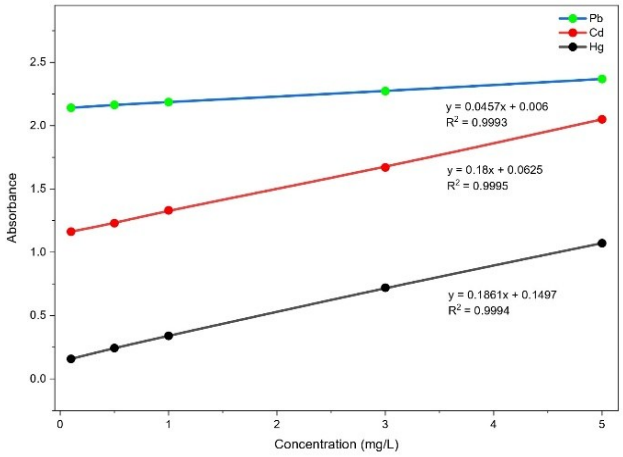

Fig. 7. Calibration curves and linear regression equations for Pb, Cd, and Hg

The observed decreasing trend in heavy metal concentrations from hESN-CP to hESN-D and subsequently to hESN-C can be attributed to differences in raw material composition and the extent of impurity removal during pre-processing. The hESN-CP, which is enriched with feather residues and co-product fractions, is more susceptible to heavy metal accumulation due to prolonged environmental exposure of feathers, which can adsorb and retain metals from air, dust, and surrounding contaminants. Partial cleaning in hESN-D reduces surface-associated impurities, leading to lower metal levels compared to hESN-CP, while thorough cleaning in hESN-C effectively removes a substantial fraction of metal-bearing particulates and residues, resulting in the lowest concentrations observed. This pattern is consistent with previous reports indicating that heavy metal contamination in ESN is primarily associated with external deposition and residual impurities rather than the nest matrix itself [25,26].

Overall, the elemental profiles confirm that heavy metal content in ESN co-product hydrolysates is predominantly influenced by regional environmental conditions, swiftlet habitat characteristics [41], and the initial condition of raw materials, particularly the presence of feathers and surface impurities, which contribute to the higher metal levels observed in hESN-CP compared to hESN-D and hESN-C. Crucially, the compliance of all samples with China's standard limits demonstrates that the UAEH process did not promote heavy metal enrichment during hydrolysis, while freeze-drying effectively maintained the physicochemical stability of the resulting hydrolysates [11,25,26]. These results support the safety and commercial viability of UAEH-processed ESN co-products for international trade and functional food applications.

3.11. Particle size analysis (PSA)

Particle size distribution analysis, presented in Fig. 8(a) and Fig. 8(b), revealed that all UAEH-processed ESN co-product hydrolysates exhibited nanoscale particle sizes with polydispersity index (PI) values below 0.3, indicating a highly homogeneous size distribution, a key physicochemical

characteristic directly relevant to the bioavailability and biological functionality of the hydrolysates.

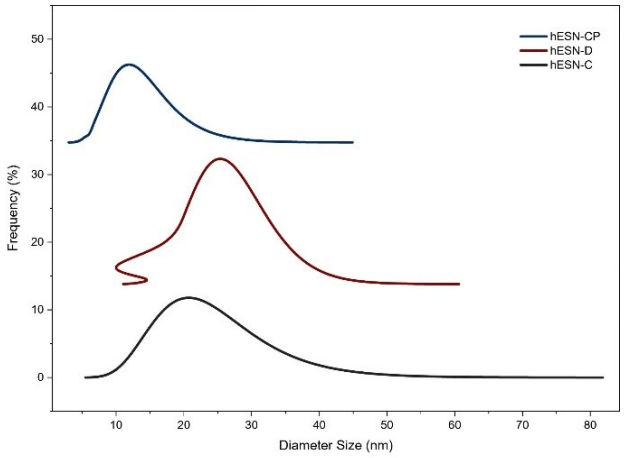

(a)

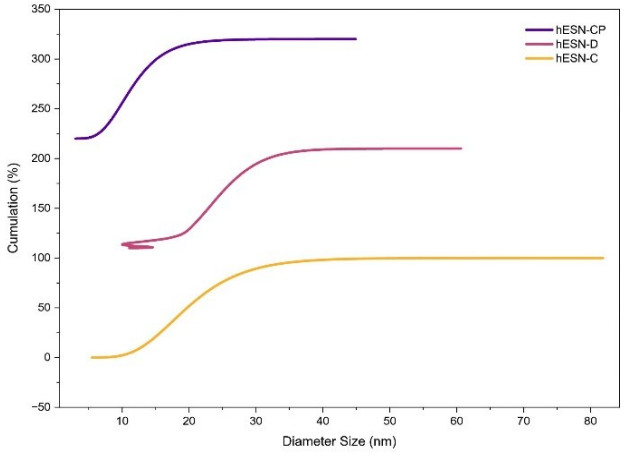

(b)

Fig. 8. Results analysis (a) particle size distribution (b) Cumulative particle size distribution of hESN-C, hESN-D, hESN-CP

As observed in the frequency distribution curves in Fig. 8(a), each hydrolysate sample displayed a distinct unimodal distribution profile, with peaks concentrated within the sub-50 nm range, confirming the predominance of nanosized particles across all three grades. The hESN-CP sample exhibited the sharpest and tallest frequency peak, with its apex occurring at the lowest diameter range (approximately 10-20 nm), indicative of the most uniform and extensively fragmented particle population among all samples. In contrast, hESN-C displayed a broader distribution peak centered at approximately 20-35 nm, while hESN-D demonstrated an intermediate distribution with a peak positioned between those of hESN-C and hESN-CP, suggesting moderate fragmentation with acceptable monodispersity. The cumulative particle size distribution curves in Fig. 8(b) further corroborate these observations: hESN-CP reached cumulative saturation at the lowest diameter threshold, followed by hESN-D and hESN-C, reflecting the progressive differences in particle size across grades. Notably, hESN-CP and hESN-D displayed steeper cumulative curves with earlier plateau formation, consistent with narrower size distributions and lower polydispersity relative to hESN-C.

In quantitative terms, hESN-C presented an average diameter (D~av~) of 24.46 nm with D10 = 12.8 nm, D50 = 19.69 nm, and D90 = 30.17 nm, and a PI of 0.1182, suggesting that the majority of particles were distributed within the lower nanometer range. The hESN-D exhibited a slightly larger average diameter of 27.03 nm (D10 = 18.46 nm, D50 = 24.11 nm, D90 = 31.66 nm) while maintaining the lowest PI of 0.0442, indicating the most monodisperse system among all samples. hESN-CP displayed the smallest particle size, with a D~av~ of 14.17 nm (D10 = 7.29 nm, D50 = 11.32 nm, D90 = 17.60 nm) and a PI of 0.1242, demonstrating the most extensive structural fragmentation, likely attributable to the keratin-rich co-product composition, which may undergo more intensive disruption during UAEH processing.

These physicochemical outcomes are mechanistically explained by the dual action of UAEH. Enzymatic hydrolysis by bromelain cleaves large glycoprotein molecules into smaller glycopeptides [12], while ultrasonic cavitation generates intense shear forces and microjets that physically disrupt protein aggregates, increase accessible surface area, and promote the formation of well-dispersed, nanosized particles [42]. The synergistic combination of these two mechanisms in UAEH thus facilitates extensive protein fragmentation and nanoscale particle formation, consistent with the frequency distribution profiles observed in Fig. 8(a), where all hydrolysate samples display narrow, well-defined peaks within the sub-50 nm range. This trend aligns with the mechanism reported for dynamic high-pressure microfluidization (DHPM), in which shear-induced de-aggregation shifts particle distribution toward lower diameters [43]. Previous studies on ESN have also reported nanosized particles (<100 nm) attributed to swollen mucinous glycoproteins (MUC5AC), confirming that ESN-derived materials inherently tend to form nanoscale structures during hydrolytic processing [44,45].

It should be noted that the present study evaluated UAEH as an integrated processing strategy, with the non-hydrolyzed raw ESN samples serving as the baseline reference for each grade. The independent contribution of ultrasound-only (UAE) and enzymatic hydrolysis-only (EAE) treatments to the observed particle size reduction was not within the scope of this study, as the synergistic superiority of UAEH over individual treatments has been previously established in the literature [2,17]. Future studies are recommended to systematically compare UAE-only, EAE-only, and UAEH treatment arms across ESN grades to further deconvolute the individual mechanistic contributions of each processing modality, particularly for co-product fractions.

From a bioactivity perspective, the nanoscale particle sizes and low polydispersity indices observed across all three hydrolysates in Fig. 8 are of particular functional significance. Nanoparticles in this size range exhibit enhanced interfacial reactivity and accessibility within gastrointestinal environments, which may positively influence digestibility, absorption efficiency, and bioactive peptide interactions with intestinal epithelial surfaces [44,45]. The cumulative distribution profiles in Fig. 8(b), showing early saturation at low diameter thresholds for hESN-CP and hESN-D, further suggest superior dispersibility characteristics in aqueous media

for these grades. Collectively, the nanoscale physicochemical properties achieved through UAEH processing are directly consistent with the enhanced soluble protein content and antioxidant activity reported in Sections 3.7 and 3.9, supporting the integrated interpretation that UAEH effectively transforms ESN co-product materials into functionally superior bioactive hydrolysates with high potential for application in functional food and nutraceutical formulations.

3.12. Scanning electron microscopy (SEM)

As shown in Fig. 9, SEM micrographs of three types of hydrolysates, each exhibiting distinct morphological characteristics according to differences in raw material sources, observed at magnifications of 500×, 1,000×, 10,000×, and 30,000×. Based on these results, the freeze-drying method clearly influences the morphological structure of the resulting particles. The hESN-C and hESN-D samples exhibit similar morphologies, characterized by the formation of flat, plate-like particles with relatively smooth surfaces and homogeneous structures. These results reveal a layered (laminar) structure typical of freeze-dried products. This observation is consistent with Dong et al. (2022) and Yeo et al. (2023), who reported that freeze-dried ESN hydrolysates tend to possess flaky structures and larger particles, possibly due to the absence of strong mechanical forces, such as shear or atomization forces, capable of breaking frozen liquids into fine droplets during the freeze-drying process [46,11]. Consequently, the solid structures formed tend to retain flake-like shapes or large aggregates.

In contrast, hESN-CP exhibits a significantly different structure. This difference is attributed to the presence of keratin in swiftlet feathers, supported by the study of Rahayu et al. (2024), which reported that swiftlet feathers contain approximately 81% keratin protein [23]. At 1,000× magnification, more complex particle aggregation and heterogeneity are observed. At higher magnifications (10,000× and 30,000×), the morphology appears irregular, with rough surfaces, the formation of small spherical particles unevenly distributed, as well as the presence of cracks and micro-pores. These characteristics indicate that hydrolysis proceeded effectively, breaking down the original feather structure into hydrolysate fractions that no longer retain the fibrillar form of keratin.

Based on SEM analysis, hESN-C and hESN-D offer the advantage of more homogeneous morphologies with layered structures and smooth surfaces, reflecting particle stability and indicating that protein bond cleavage by bromelain occurred effectively without disrupting structural uniformity. Meanwhile, hESN-CP demonstrates a higher degree of protein degradation, as evidenced by its more heterogeneous and porous surface, indicating the effectiveness of bromelain in cleaving protein bonds in keratin-rich ESN co-products.This observation is consistent with the findings reported by Tai et al. (2020), who reported that bromelain is capable of breaking protein bonds [17]. Therefore, it can be concluded that hESN-CP generally produce more heterogeneous and porous surfaces, whereas hESN-C and hESN-D exhibit more homogeneous surfaces.

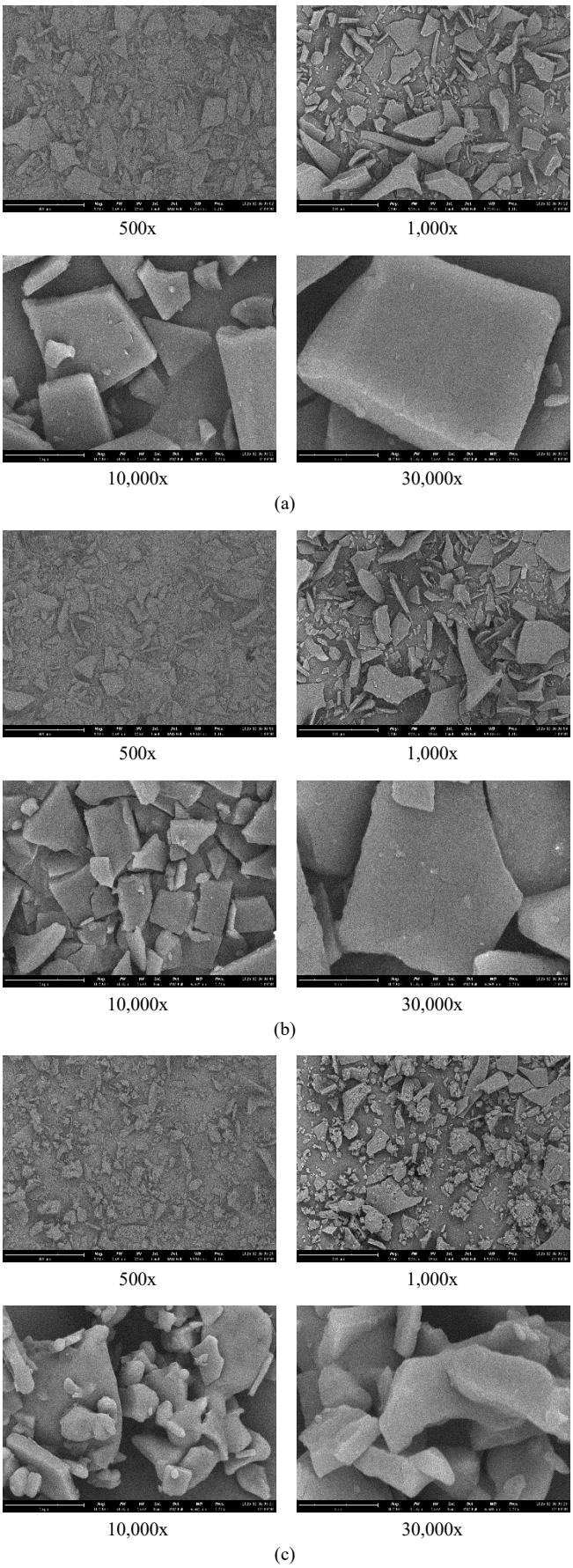

Fig. 9. SEM analysis of (a) hESN-C, (b) hESN-D, (c) hESN-CP

3.13. Whiteness index

The whiteness (L^*) values of freeze-dried UAEH-processed ESN co-product hydrolysates are presented in Table 9. Significant differences in L^* were observed among most sample pairs ($p < 0.05$), with the exception of hESN-D and hESN-CP ($p \leq 0.05$). The hESN-C hydrolysate exhibited the highest L^* value (37.00 ± 0.20), while hESN-CP showed the lowest (31.37 ± 0.38), reflecting the influence of co-product composition on the color characteristics of the resulting hydrolysates.

Table 9. Whiteness values of each raw material and its freeze dried product

Samples	Whiteness (L^*)
ESN-C	63.53 ± 1.14a
ESN-D	26.27 ± 1.17b
ESN-CP	3.90 ± 0.56c
hESN-C	37.00 ± 0.20d
hESN-D	33.37 ± 0.78e
hESN-CP	31.37 ± 0.38e

Different superscript letters denote significant differences ($p < 0.05$)

Notably, UAEH substantially reduced the large L^* differences observed in the unprocessed raw materials. The raw ESN-C and ESN-CP exhibited a mean L^* difference of 32.17, whereas the corresponding freeze-dried UAEH hydrolysates showed a markedly reduced mean difference of only 5.63, demonstrating the homogenizing effect of the UAEH process on the physicochemical color properties of ESN co-product hydrolysates. Similarly, the L^* difference between raw ESN-D and ESN-CP was 22.37, yet no significant difference in whiteness was detected between hESN-D and hESN-CP ($p \leq 0.05$), with a mean difference of only 2.17.

These findings are consistent with Ling et al. (2020), who reported that enzymatic hydrolysis reduces yellowness in raw ESN [14], and with Chantakun & Benjakul (2022), who demonstrated that ultrasonication as a pre-treatment prior to enzymatic hydrolysis significantly increases the L^* value of the resulting hydrolysate [7]. The combined application of ultrasound and enzymatic hydrolysis in the UAEH process therefore appears to synergistically improve the whiteness of ESN co-product hydrolysates, yielding products with more favorable physicochemical color attributes regardless of the initial raw material condition, a practically significant outcome for the commercial application of ESN co-product hydrolysates in functional food formulations.

3.14. Water activity

The water activity (aw) values of ESN raw materials and their UAEH-processed hydrolysates are presented in Table 10. Among unprocessed samples, ESN-D exhibited the significantly highest aw (0.66 ± 0.01), followed by ESN-C (0.63 ± 0.01) and ESN-CP (0.59 ± 0.01). Following UAEH processing and freeze-drying, all hydrolysates demonstrated reduced aw values: hESN-C (0.59 ± 0.01), hESN-D (0.54 ± 0.01), and hESN-CP (0.52 ± 0.01).

Table 10. Water Activity of ESN

Samples	Water Activity
ESN-C	0.63
ESN-D	0.66
ESN-CP	0.59
hESN-C	0.59
hESN-D	0.54
hESN-CP	0.52

The aw values of ESN-CP and all UAEH-processed hydrolysates (hESN-C, hESN-D, and hESN-CP) were consistently below 0.60, a critical physicochemical threshold below which microbial growth is effectively suppressed and biochemical deterioration is minimized [3,47]. This confirms that UAEH processing combined with freeze-drying successfully produced ESN co-product hydrolysates with favorable stability characteristics. A significant difference ($p < 0.05$) was observed between unprocessed and UAEH-processed samples, confirming that the combined treatment effectively reduced water activity across all co-product types.

Among all hydrolysates, hESN-CP achieved the lowest aw (0.52 ± 0.01), indicating the highest physicochemical stability and shelf life potential. This outcome can be attributed to the combined effect of enzymatic hydrolysis, which extensively disrupted the co-product protein matrix, including keratin-rich fractions, and the subsequent freeze-drying step, which efficiently removed residual moisture. Conversely, unprocessed ESN-C and ESN-D, with aw values exceeding 0.60, are considered shelf-unstable and microbiologically unsafe without further processing. Overall, these results demonstrate that UAEH processing is an effective strategy for improving the physicochemical stability of ESN co-product hydrolysates, with hESN-CP representing the most stable product suitable for long-term storage and functional food applications.

4. Conclusion

This study demonstrates that ultrasound-assisted enzymatic hydrolysis (UAEH) is an effective strategy for valorizing edible swiftlet nest co-products (ESN-CP). UAEH significantly enhanced soluble protein content, yielded nanoscale particles with low polydispersity indices (<0.3), and induced distinct morphological transformations in the glycoprotein matrix, as confirmed by SEM. FTIR analysis verified the preservation of characteristic amide and glycan-associated functional groups, while qualitative HPLC profiling detected sialic acid across all hydrolysate samples, consistent with the protease-exclusive specificity of bromelain. UAEH treatment further produced a statistically significant increase in DPPH radical scavenging activity compared to raw material controls across all ESN grades ($p < 0.05$), although the observed inhibition values (10.70-16.12% at 100 ppm) should be interpreted as preliminary in vitro indicators pending further bioactivity validation. Heavy metal contents in all samples remained below applicable regulatory thresholds (Hg ≤ 0.05, Cd ≤ 1, Pb ≤ 2 ppm), and water activity values below 0.60 confirm the physicochemical stability of the freeze-dried hydrolysates. Collectively, these findings establish a scientific basis for the

valorization of ESN co-products into functional ingredient candidates. Future studies should prioritize quantitative sialic acid determination, multi-assay antioxidant profiling, and in vitro or in vivo bioactivity validation to substantiate functional food applications.

Acknowledgements

The authors acknowledge the financial support provided by the Ministry of Education, Culture, Research, and Technology of the Republic of Indonesia through the Matching Fund Research Scheme.

References

1. R. N. Afifah, S. L. Hendrawan, B. Ramadhani, A. C. D. Rahmadhani, N. R. Shafitri, A. H. Tsana, F. A. Wahyudi, P. Setiarso, N. Kusumawati, M. T. Asri, and S. Kuntjoro. *Effectiveness of voltammetry and UV-Vis spectrophotometry methods in analyzing nitrite in edible swiftlet nest*. Rasayan J. Chem. 17(3) (2024) 1141–1145.
2. R. Waskito, K. Rahmawati, N. Hidayah, F. F. Fachrirakarsie, N. H. Putri, K. Z. R. Maulida, and P. Setiarso. *The effect of ascorbic acid on nitrite and peroxide levels and nutritional content of edible swiftlet's nest*. Rasayan J. Chem. 16(4) (2023) 2340–2344.
3. J. Y. Gan, L. S. Chang, N. A. M. Nasir, A. S. Babji, and S. J. Lim. *Evaluation of physicochemical properties, amino acid profile and bioactivities of edible bird's nest hydrolysate as affected by drying methods*. LWT Food Sci. Technol. (2020) 1–25.
4. N. N. Zulkefle, M. A. Ibrahim, N. F. Azuan, S. E. Ch'ng, N. Ismail, M. Z. A. Bakar, and K. W. Chan. *A review on the edible bird's nest quality and manufacturing standards of the three largest exporting countries in the world*. J. Food Qual. (2024) 1–23.
5. A. F. E. Sheikha. *Why the importance of geo-origin tracing of edible bird nests is arising?*. Food Research International. 150 (2021).
6. S. P. Loh, S. H. Cheng, and W. Mohamed. *Edible bird's nest as a potential cognitive enhancer*. Front. Neurol. 13 (2022) 1–12.
7. K. Chantakun & S. Benjakul. *Effect of ultrasound-assisted pretreatment in combination with heating on characteristics and antioxidant activities of protein hydrolysate from edible bird's nest co-product*. J. Food Sci. Technol. 59(10) (2022) 3908–3917.
8. S. J. Lim, L. S. Chang, S. Fazry, W. A. W. Mustapha, and A. S. Babji.. *Functional food and ingredients from seaweed, edible bird's nest and tropical fruits: a translational research*. Food Res. Technol. 151 (2021).
9. C. H. Ng, P. L. Tang, and Y. Y. Ong. *Enzymatic hydrolysis improves digestibility of edible bird's nest (EBN): combined effect of pretreatment and enzyme.* J. Food Meas. Charact. 17 (2023) 549–563.
10. J. Qian, D. Chen, Y. Zhang, X. Gao, L. Xu, G. Guan, and F. Wang. *Ultrasound-assisted enzymatic protein hydrolysis in food processing: mechanism and parameters*. Foods. 12 (2023) 1–27.
11. B. H. Yeo, S. F. Wong, C. P. Tan, Y. Rukayadi, and O. M. Lai. *Characterization of freeze- and spray-dried edible bird's nest hydrolysates*. Int. J. Chem. Biochem. Sci. 24(7) (2023) 199–203.
12. P. L. Tang and X. J. Koh. *Ultrasound-assisted enzymatic hydrolysis enhances anti-inflammatory and hypoglycemic activities of edible bird's nest*. Food Biosci. 56 (2023) 1–10.
13. W. Y. Tham, M. K. Ong, & C. Y. Teoh. *Sialic acid, nutritional and fatty acid compositions of three species of freshwater fish eggs*. BIO Web of Conferences. 182 (2025).
14. J. W. A. Ling, L. S. Chang, A. S. Babji and S. J. Lim. *Recovery of value-added glycopeptides from edible bird's nest (EBN) co-products: enzymatic hydrolysis, physicochemical characteristics and bioactivity*. J. Sci. Food Agric. 100 (2020) 4714–4722.
15. P. K. Chong, S. L. Mun, L. S. Chang, A. S. Babji, and S. J. Lim. *Fractionation of edible bird's nest glycoprotein hydrolysates: characterisation and antioxidative activities of the fractions*. Food Sci. Hum. Wellness. 11 (2022) 886–894.
16. A. Damayanti, A. R. Hakim, and R. Saputri. *GC-MS analysis of metabolite composition in edible bird's nest from Jenamas, Central Kalimantan*. Int. J. Pharm. Appl. Health Sci. 1(1) (2023) 6–9.
17. S. K. Tai, Z. Hamzah, Q. H. Ng, and C. S. Tan. Surface morphology study on unclean, commercial and bromelain treated edible bird nest (EBN) using scanning electron microscope. IOP Conf. Ser. Mater. Sci. Eng. 932 (2020).
18. Badan Pusat Statistik. *Exports of bird's nest by major countries of destination, 2012–2024*. (2025). [Online]. Available: https://www.bps.go.id/en/statistics-table/1/MjAyMiMx/exports-of-bird-nest-by-major-countries-of-destination---2012-2024.html
19. M. M. S. Basukiwardojo, N. Kusumawati, M. T. Asri, S. A. Dzulkarnain, A. N. A. Hafidl, A. Kahfi, M. A. Nabila, F. Setiawan, L. Isyrak, and K. Rahmawati. *Ionic liquid ultrasound-assisted extraction (IL-UAE) for duck feather keratin and in silico evaluation as a potential procollagen n-endopeptidase inhibitor*. Commun. Sci. Technol. 10(1) (2025) 75–86.
20. G. Bermudez, C. Terenzi, F. Medri, V. Andrisano, and S. Montanari. *Comprehensive amino acids profiling of microalgae by gas chromatography-mass spectrometry analysis after pre-column derivatization.* J. of Food Composition and Analysis. 140 (2025) 1-11.
21. A. K. Hemker, A. Abdullah, S. Pimentel-Moral, V. M. Gómez-López and F. J. Barba. *Effects of high-pressure-assisted enzymatic hydrolysis on physicochemical and antioxidant properties of fish protein hydrolysates.* J. Food Eng. 278 (2020).
22. M. Olszwy-Tomczyk. *How to Express The Antioxidant Properties of Substances Properly?* Chemical Paper. 75 (2021) 6157-6167.
23. S. Rahayu, W. Suryapratama, F. M. Suhartati, M. Bata, E. A. Rimbawanto, and B. Hartoyo. *Quality of edible bird's nest treated by keratinolytic enzymes-based cleaning solution*. Food Res. 8(2) (2024) 299–307.
24. H. S. M. Noor, R. M. Ariff, L. S. Chang, X. Y. Chai, H. Y. Tan, N. A. Daud, A. S. Babji, and S. J. Lim. *Enzymatic recovery of glycopeptides from different industrial grades edible bird's nest and its by-products: nutrient, probiotic and antioxidant activities, and physicochemical characteristics.* Food Sci. Hum. Wellness. 11 (2022) 1555–1564.
25. R. M. Ibrahim, N. N. M. Nasir, M. Z. A, Bakar, R. Mahmud, N. A. A. Razak. *The Authentication and Grading of Edible Bird's Nest by Metabolite, Nutritional, and Mineral Profiling*. Foods. 10 (2021) 1-14.
26. C. H. Lee, N. Hamdan, B. B. Nyakuma, S. L. Wong, K. Y. Wong, H. Tan, and T. H. Lee. *Purification, identification and molecular docking studies of antioxidant and anti-inflammatory peptides from edible bird's nest*. Food Chem. 454 (2024).
27. C. H. Tung, J. Q. Pan, H. M. Chang, & S. S. Chou. *Authentic determination of bird's nests by saccharides profile*. Journal of Food and Drug Analysis. 16(4) (2008) 86–91.
28. A. Ujuldah, A. R. Hakim, and R. Saputri. *FTIR spectroscopic characterization of edible bird's nest from Jenamas, Central Kalimantan.* Int. J. Pharm. Appl. Health Sci. 1(1) (2023) 1–5.
29. M. H. Wang, Z. F. Wang, C. G. Yang, D. L. Wang, & S. Q. Wang. *Changes in the Serum and Tissue Levels of Free and Conjugated Sialic Acids, Neu5Ac, Neu5Gc, and KDN in Mice after the Oral Administration of Edible Bird's Nests: An LC–MS/MS Quantitative Analysis*. Separations. 107 (2024).
30. T. Dighriri, M. Aljofan, and A. S. Alshammari. *Omega-3 polyunsaturated fatty acids and their role in brain functions: A systematic review*. J. Food Biochem. 46(4) (2022) e14123.
31. S. Shaninfar, M. R. Goli, and M. Rezaei. *Bioactive compounds and fatty acid profile of edible bird's nest: Functional and nutritional perspectives*. J. Ethn. Foods 12 (2025) 15.
32. T. H. Lee, W. A. Wani, C. H. Lee, N. A. Azmi, S. Kavita, M. Znati, and H. B. Jannet. Characterization of polar and non-polar compounds and bioactivity of edible bird's nest from Johor, Malaysia. Chem. Biodiversity (2020).
33. O. Mahaq, H. A. Hassim, M. H. M. Noor, N. Titisari, & H. Ahmad. *Effects of dietary edible bird's nest supplementation on hippocampal neurons of multigenerational mice*. International Journal of Biosciences. 3(3) (2024) 33-46..
34. R. Mohamad Ibrahim, N. N. Mohamad Nasir, M. Z. Abu Bakar, R. Mahmud, and N. A. Ab Razak. *The authentication and grading of edible bird's nest by metabolite, nutritional, and mineral profiling.* Foods. 10 (2021) 1574.
35. N. N. Mohamad Nasir, R. Mohamad Ibrahim, M. Z. Abu Bakar, R. Mahmud, and N. A. Ab Razak. *Characterization and extraction influence protein profiling of edible bird's nest. Foods*. 10 (2021) 2248.
36. D. D. Murugan, Z. M. Zain. K. W. Choy, N. H. Zamakshshari, M. J. Choong, Y. M. Lim, & M. R. Mustafa. *Edible Bird's Nest Protects Against Hyperglycemia-Induced Oxidative Stress and Endothelial Dysfunction*. Frontiers in Pharmacology. 10 (2020).
37. T. T. Nguyen, H. Q. Pham, N. T. L. Tran, and D. V. Nguyen. *Fatty acid composition and bioactive properties of edible bird's nest hydrolysates*. Food Chem. 402 (2024) 134215.
38. P. L. Tang, H. S. Goh, and S. S. Sia. *Combined enzymatic hydrolysis and herbal extracts fortification to boost in vitro antioxidant activity of edible*

bird's nest solution. Chinese Herbal Medicines 13 (2021) 549–555.
39. C. Wen, J. Zhang, J. Zhou, M. Cai, Y. Duan, H. Zhang, H. Ma. *Antioxidant Activity of Arrowhead Protein Hydrolysatees Produces by a a Novel Multi-Frequency S-Type Ultrasound-Assisted Enzymolysis.* Natural Product Research. 34 (2020) 3000-3003.
40. B. H. Yeo, T. K. Tang, S. F. Wong, L. Z. Cheong, and O. M. Lai. *Potential Residual Contaminants in Edible Bird's Nest*. Front. Pharmacol. 12 (2021) 1-15.
41. M. C. Quek, N. L. Chin, Y. A. Yusof, C. L. Law, S. W. Tan. *Characterization of edible bird's nest of different production, species and geographical origins using nutritional composition, physicochemical properties and antioxidant activities*. Food Res. Int. (2018) 1-42.
42. S. S. P. Perdana, N. Kusumawati, M. M. S. Basukiwardojo, P. Setiarso, G. N. Djalilah, and K. Rahmawati. *The effect of ultrasonication on the quality of keratin extraction based on ionic liquid from duck feather*. Commun. Sci. Technol. (2025) 1–8.
43. Q. Fan, P. Wang, X. Zheng, S. S. Hamzah, H. Zeng, Y. Zhang, and J. Hu. *Effect of dynamic high pressure microfluidization on the solubility properties and structure profiles of proteins in water-insoluble fraction of edible bird's nests*. LWT Food Sci. Technol. 132 (2020) 1–8.
44. M. N. G. Amin, G. Soegiarto, and L. Wulandari. *The physicochemical and antioxidant activity of Realfood' hydrolysed bird nest (RHBN)*. Appl. Food Res. 5 (2025) 1–7.
45. A. S. Babji, M. H. Nurfatin, I. K. E. Syarmila, & M. Masitah. *Secrets of edible bird nest*. UTAR Agriculture Science Journal. 1 (2015) 32–37.
46. Y. Dong, W. Yan, and Y. Q. Zhang. *Effects of Spray Drying and Freeze Drying on Physicochemical Properties, Antioxidant and ACE Inhibitory Activities of Bighead Carp (Aristichthys nobilis) Skin Hydrolysates.* Foods. 11(14) (2022) 1-13.
47. L. S. Chang, R. Karim, A. Sabo Mohammed and H. Mohd Ghazali. *Production and characterization of enzyme-treated spray-dried soursop (Annona muricata L.) powde*r. J. Food Process Eng. 41 (2018).